Ridge subduction at an erosive margin: The collision zone of the Nazca Ridge in southern Peru

Andrea Hampel[1] and Nina Kukowski
GeoForschungsZentrum Potsdam, Potsdam, Germany

Joerg Bialas
GEOMAR Research Center for Marine Geosciences, Kiel, Germany

Christian Huebscher and Raffaela Heinbockel
Institut fuer Geophysik, Universitaet Hamburg, Hamburg, Germany

Received 19 May 2003; revised 31 October 2003; accepted 18 November 2003; published 3 February 2004.

[1] The 1.5-km-high, obliquely subducting Nazca Ridge and its collision zone with the Peruvian margin have been imaged by wide-angle and reflection seismic profiles, swath bathymetry, and gravity surveying. These data reveal that the crust of the ridge at its northeastern tip is 17 km thick and exhibits seismic velocities and densities similar to layers 2 and 3 of typical oceanic crust. The lowermost layer contributes 10–12 km to the total crustal thickness of the ridge. The sedimentary cover is 300–400 m thick on most parts of the ridge but less than 100 m thick on seamounts and small volcanic ridges. At the collision zone of ridge and margin, the following observations indicate intense tectonic erosion related to the passage of the ridge. The thin sediment layer on the ridge is completely subducted. The lower continental slope is steep, dipping at $\sim 9^\circ$, and the continental wedge has a high taper of 18°. Tentative correlation of model layers with stratigraphy derived from Ocean Drilling Program Leg 112 cores suggests the presence of Eocene shelf deposits near the trench. Continental basement is located <15 km landward of the trench. Normal faults on the upper slope and shelf indicate extension. A comparison with the Peruvian and northern Chilean forearc systems, currently not affected by ridge subduction, suggests that the passage of the Nazca Ridge along the continental margin induces a temporarily limited phase of enhanced tectonic erosion superposed on a long-term erosive regime. *INDEX TERMS:* 3025 Marine Geology and Geophysics: Marine seismics (0935); 3045 Marine Geology and Geophysics: Seafloor morphology and bottom photography; 8015 Structural Geology: Local crustal structure; 8105 Tectonophysics: Continental margins and sedimentary basins (1212); 8122 Tectonophysics: Dynamics, gravity and tectonics; *KEYWORDS:* ridge subduction, tectonic erosion, active Peruvian margin, forearc structure, wide-angle seismics, reflection seismics

Citation: Hampel, A., N. Kukowski, J. Bialas, C. Huebscher, and R. Heinbockel (2004), Ridge subduction at an erosive margin: The collision zone of the Nazca Ridge in southern Peru, *J. Geophys. Res.*, *109*, B02101, doi:10.1029/2003JB002593.

1. Introduction

[2] Seamount chains, submarine ridges, and other bathymetric highs on oceanic plates entering subduction zones may significantly affect the sedimentological and tectonic evolution of forearc systems. The response of the forearc system to the subduction of a bathymetric high depends on whether the long-term mass transfer regime at the margin has been dominated by accretion or tectonic erosion. At primarily accretive margins, subducting bathymetric highs cause, in general, large indentation and partial removal of the accretionary prism [*Chung and Kanamori*, 1978; *McCann and Habermann*, 1989; *Bouysse and Westercamp*, 1990; *Lewis et al.*, 1995; *Lallemand et al.*, 1994; *von Huene et al.*, 1997; *Dominguez et al.*, 1998; *Schnuerle et al.*, 1998; *Behrmann and Kopf*, 2001]. In the wake of a subducted bathymetric high, an accretionary wedge grows again, given sufficient sediment supply from the oceanic plate. At margins dominated by subduction erosion, the increased rate of erosion caused by subducting ridges may not be clearly distinguishable from the unaffected or long-term background state and therefore more difficult to quantify. Depending on the shape of the subducting bathymetric high and the structure of the forearc and coastal region, the slope and shelf regions may be less deeply indented than at an primarily accretive margin. The most pronounced effects are uplift and steepening of the forearc, which may be documented in the offshore and onshore sedimentological record [e.g., *Vogt et al.*, 1976; *McCann and Habermann*, 1989;

[1]Now at Institute of Geological Sciences, University of Berne, Berne, Switzerland.

0148-0227/04/2003JB002593$09.00

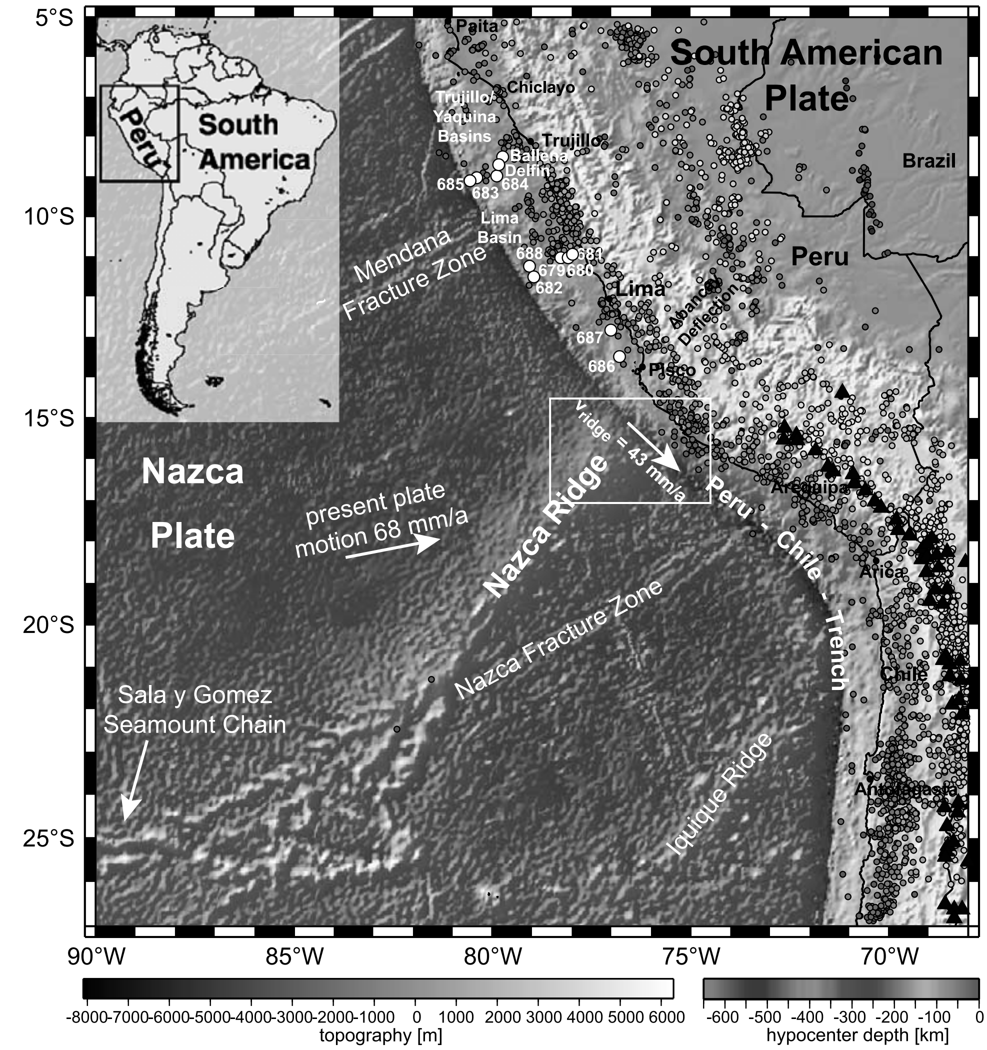

Figure 1. Topographic map of the Nazca Ridge and the South American margin [*Smith and Sandwell*, 1997]. Relative plate motion of the Nazca plate is taken from *Norabuena et al.* [1998], trench-parallel motion of the Nazca Ridge from *Hampel* [2002]. Colored circles represent earthquakes recorded from 1973 to 2002 (from the U.S. Geological Survey, National Earthquake Information Center). Note the gap in the intermediate depth seismicity (70–300 km) and the presence of deep seismic events (500–650 km) beneath Brazil, both phenomena in the presumed linear continuation of the ridge. Active volcanic centers are marked by black triangles (from the Smithsonian Global Volcanism Program). Locations of ODP Leg 112 sites and two industrial wells (Ballena, Delfin) are indicated by white circles. See color version of this figure in the HTML.

Corrigan et al., 1990; *Gardner et al.*, 1992; *Lallemand et al.*, 1992; *Collot and Davy*, 1998; *Ranero and von Huene*, 2000; *Spikings et al.*, 2001]. Furthermore, the subduction of an elongated bathymetric high may lead to a temporal sequence forearc uplift followed by subsidence, because the underthrusting ridge commonly migrates along the active margin owing to its oblique orientation to the convergence direction of the oceanic plate [*Dupont*, 1982; *Dupont and Herzer*, 1985; *LeFevre and McNally*, 1985; *Ballance et al.*, 1989; *McCann and Habermann*, 1989; *Fisher et al.*, 1991; *Collot and Fisher*, 1991; *Lallemand et al.*, 1992; *Cloos*, 1993; *von Huene et al.*, 1997; *Dominguez et al.*, 1998; *Schnuerle et al.*, 1998; *Laursen et al.*, 2002]. Only where the ridge is orientated orthogonally with respect to both plate convergence direction and margin, the collision zone remains stationary and tectonic manifestation of the collision may include a coastal thrust belt [*Geist et al.*, 1993; *Geist and Scholl*, 1994; *Kolarsky et al.*, 1995].

[3] A quantification of the effects of ridge subduction benefits from settings where the influence of ridge subduction can be compared to adjacent unaffected areas. Such a favorable setting is provided at the Peruvian active margin, where the Nazca Ridge subducts beneath the South American continent. The collision zone of the Nazca Ridge has migrated southward along the Peruvian margin during the Cenozoic to reach its present location at 15°S (Figure 1) [*Pilger*, 1981; *Cande*, 1984; *von Huene and Lallemand*, 1990; *von Huene et al.*, 1996; *Hampel*, 2002]. With respect to the dominating process of mass transfer, the Peruvian margin north of ~10°S has been classified as tectonically erosive [*Rutland*, 1971; *Scholl et al.*, 1970], whereas an active primarily accretive regime has been suggested south

of ~11°S off central Peru [*von Huene and Lallemand*, 1990; *von Huene et al.*, 1996]. Recent studies, however, advocate a dominantly erosive regime for the central and southern Peruvian margin [*Kukowski et al.*, 2001b; *Clift et al.*, 2003].

[4] The aim of this study is to report our investigation of the structure of the Nazca Ridge and the present collision zone with the southern Peruvian margin. We present new multibeam bathymetric, gravity, wide-angle, and reflection seismic data collected during cruise SO146 of the German R/V *Sonne* from March to May 2000, which give insights into the morphology, the crustal structure, and the mass transfer regime of the active collision zone.

2. Geodynamic Setting

[5] The 200-km-wide, N42°E trending submarine Nazca Ridge extends more than 1100 km across the southeast Pacific seafloor (Figure 1). Its crest rises 1500 m above the surrounding seafloor and resides above the carbonate compensation depth. The flanks of the ridge dip gently at 1–2° [*Hagen and Moberly*, 1994]. Because of a thick lower crustal layer revealed by gravity data [*Couch and Whitsett*, 1981] the crust of the ridge is at least twice as thick as the crust of the adjacent Nazca plate. Analysis of earthquake waves yielded an average crustal thickness of the ridge of 18 ± 3 km [*Woods and Okal*, 1994]. The Nazca Ridge, whose oldest not yet subducted part is of early Tertiary age, formed at the Pacific-Farallon/Nazca spreading center in the Cretaceous [*Pilger and Handschumacher*, 1981; *Pilger*, 1981; *Woods and Okal*, 1994] and has a common origin with the Tuamotu Plateau, which represents its conjugate feature on the Pacific plate [*Pilger*, 1981].

[6] Where the ridge intersects the margin, the trench axis shallows. However, the collision is not expressed as a large reentrant at the base of the margin. Bathymetric and side-scan sonar images reveal ongoing surface erosion and faulting on the continental slope [*Hussong et al.*, 1988; *Hagen and Moberly*, 1994; *Li and Clark*, 1994]. Between 13.5°S and 17°S, the continental shelf narrows above the subducted ridge, and the coastline is shifted westward. Forearc uplift is recorded by marine terraces and by Eocene to upper Pliocene marine deposits that have been raised above sea level [*Hsu*, 1992; *Macharé and Ortlieb*, 1992]. Parts of the coastal cordillera consist of the formerly submarine transition zone between continental shelf and slope [*Hsu*, 1992]. Three of the several strong interplate earthquakes that ruptured beneath Peru in the past decades have nucleated along the downdip projection of the Nazca Ridge [*Spence et al.*, 1999; *Swenson and Beck*, 1999]. The earthquakes of 1942 and 1996 with magnitudes M_w = 8.1 and M_w = 7.7, respectively, were located above the subducted crest and southeastern flank of the ridge. In 2001, another earthquake with a magnitude of M_w = 8.4 and several aftershocks of magnitude M_w = 6.0 and larger ruptured the coastal area at the southern edge of the subducted ridge.

3. Data Acquisition and Processing

[7] During R/V *Sonne* cruise SO146-GEOPECO, multibeam swath bathymetry was collected between 14°S and 17°S (Figures 2–4) using the onboard Hydrosweep system [*Grant and Schreiber*, 1990]. These data were edited and processed with the MB-System software package [*Caress and Chayes*, 1995]. Spatial resolution is ~200 m at 6000 m water depth. SO146-GEOPECO cruise data have been compiled with bathymetry extracted from side-scan sonar data acquired by Hawaii Institute of Geophysics (HIG), in 1987 [*Hussong et al.*, 1988; *Hagen and Moberly*, 1994; *Li and Clark*, 1994].

[8] Two crossing wide-angle seismic refraction and reflection profiles were acquired using GEOMAR ocean bottom hydrophones (OBH) [*Flueh and Bialas*, 1996] and three-component ocean bottom seismometers (OBS) [*Bialas and Flueh*, 1999] as receivers (Figure 2). Along the 175-km-long profile SO146-01 shot perpendicular to the Nazca Ridge, six OBHs and three OBSs were symmetrically positioned around station OBS05. This instrument was also used as the westernmost station for profile SO146-02 positioned along the ridge crest (Figure 2). On this line, which extends eastward to the continental shelf, three other OBS and ten OBH instruments were deployed. For both profiles, an array of three 32 1 Bolt air guns generated the seismic signal every 60 seconds, resulting in a shot distance of 120 m. The reflection arrivals were additionally recorded by a single-channel streamer (Figure 5; profiles HH-01, HH-02). To achieve higher resolution, a shorter multichannel seismic line (HH-03), coincident with the northeastern part of profile SO146-02 that crosses the trench and continental slope, was acquired using two GI air guns firing every 20 m (Figure 6).

[9] The majority of the OBH/OBS instruments, in particular the stations located on the oceanic crust and on the lower slope, recorded high-quality data with the exception of the seismometer of OBS05 and three OBHs on ridge-parallel profile SO146-02. Most instruments including the hydrophone of OBS05 show clear signals to large offsets, some over the entire profile length and offset distances as much as ~140 km (Figures 7 and 8). All stations on ridge-crossing profile SO146-01 and most SO146-02 stations show pronounced wide-angle reflections (*PmP*) at large offsets related to the crust-mantle boundary. These arrivals tightly constrain the location of the Moho. Stations located on the shelf have a higher noise level than those located more seaward.

[10] Processing of the wide-angle seismic data included frequency filtering and deconvolution. To derive the final velocity models of both profiles, all available OBH/OBS records were used. The two single-channel reflection profiles and a stacked section of the multichannel reflection profile provided information about the morphology of the sediment layers and crystalline crust and additionally constrained the velocity models. Forward modeling by ray tracing was carried out using programs by *Luetgert* [1992] and *Zelt and Smith* [1992]. The two profiles were correlated by OBS05 station (Figure 9). Ray coverage is good for both profiles, despite the three missing records on SO146-02 (Figure 10). The uncertainty in the location of the model layers is ~100 m and ~800 m for the lower and upper layers, respectively. A good fit between observed and calculated travel times was achieved with time differences not exceeding 0.3 s in the near-offset and 0.5 s in the far-offset arrivals (Figures 11 and 12).

[11] Gravity readings were recorded every 10 s during the entire cruise using the air-sea gravity meter KSS 30/31 15 of the Bodenseewerke Geosystem GmbH. After applying an Eotvos correction, a correction of the latitude dependency

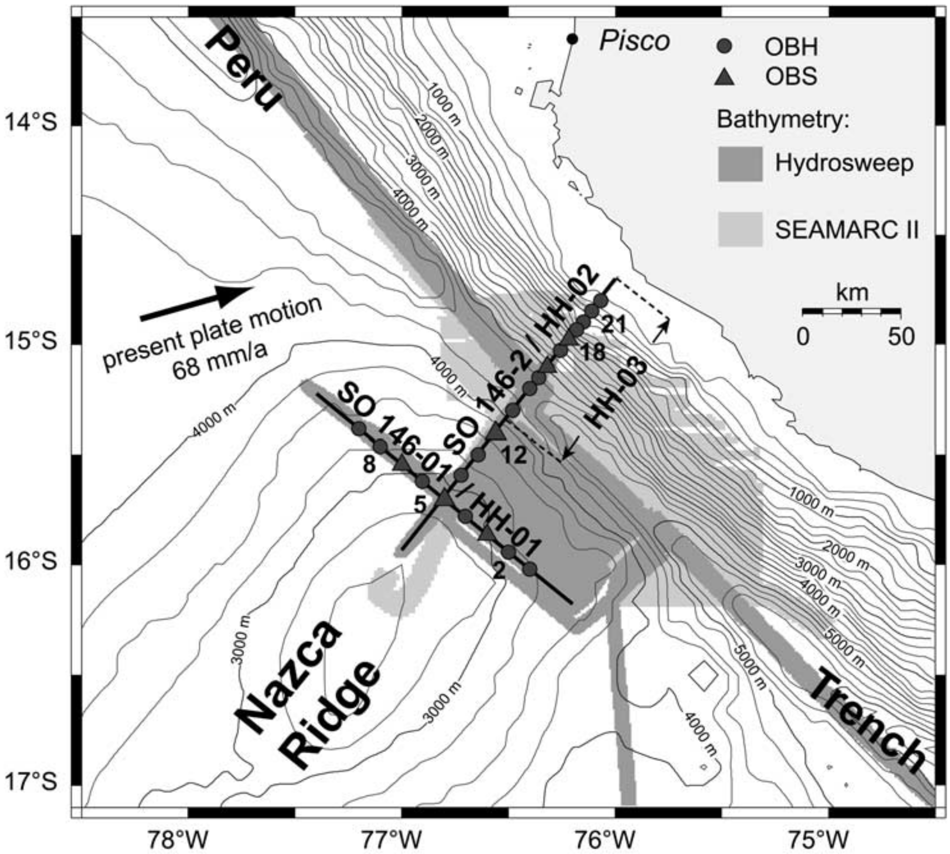

Figure 2. Location map of the Nazca Ridge at the intersection with the Peru Trench. Wide-angle seismic profiles SO146-01 and SO146-02 coincide with seismic reflection lines HH-01, HH-02, and HH-03. Areas shaded in dark and light grey were covered by Hydrosweep (this cruise) and SEAMARC II (acquired by the Hawaii Institute of Geophysics) bathymetry, respectively.

and of errors caused by strong acceleration or turns of the ship, the data were compiled with navigation information and *GEODAS* [1992] data. In this paper, we present the underway gravity data coincident with the wide-angle seismic line SO146-02, for which the density model was derived by using the software IGMAS (Figure 13) [*Goetze and Lahmeyer*, 1988] and constraints provided by the seismic velocity model (compare Figures 10b and 13). The uncertainty of the gravity measurements is better than 10^{-5} m/s^2; observed and calculated values are in good agreement (Figure 13).

4. Data Interpretation

4.1. Nazca Ridge

[12] On the southeastern flank of the Nazca Ridge, several prominent volcanic edifices have been imaged by bathymetry (Figure 3). An ~800-m-high seamount with a diameter of ~20 km is located in the center of the mapped area (Figure 3, box 1). Another 400-m-high seamount with a well-preserved caldera ~4 km in diameter and several conical structures lie near the crest of the Nazca Ridge (Figure 3, box 2). Two 20- to 30-km-long volcanic ridges occur adjacent to the two seamounts, one 500 m high between them and the other of 1100 m height south of the larger southern seamount (Figure 3).

[13] The sedimentary cover on the ridge is 300–400 m thick except on the volcanic edifices where the thickness of the sediment is reduced to tens of meters (Figure 5). Near the crest of the ridge, wide-angle and vertical seismic reflection profiles cross the seamount-crested caldera and reveal its internal structure (Figure 5a). Along the crest of the ridge, four basement highs occur west of the trench axis (Figure 5b). Sill layers flanking one of these are imaged within the sedimentary cover.

[14] Forward modeling of the wide-angle seismic data (Figures 9 and 11) yields a velocity between 1.6 and 1.8 km/s for the oceanic sediment layer A_{oc}. Seismic velocity increases rapidly in the upper crust, within which three different layers (B_{oc}–D_{oc}) can be distinguished. Layers B_{oc}–D_{oc} exhibit velocity gradients of 3.5–3.9, 4.5–5.0, and 5.2–5.7 km/s, respectively (Figure 9). Gravity modeling yields corresponding densities of 2500, 2700, and 2800 kg/m^3 (Figure 13). The lower part of the crust is modeled as a ~2-km-thick layer (E_{oc}) with a velocity gradient of 6.2–6.6 km/s and a ~10-km-thick layer (F_{oc}) with a gradually increasing velocity of 6.7–7.5 km/s (Figure 9). Layers E_{oc} and F_{oc} show densities of 2910 and 2980 kg/m^3, respectively (Figure 13). Layer F_{oc} constitutes more than half of the entire crustal thickness (Figure 9). The total thickness of layers B_{oc}–E_{oc} of 4–5 km slightly increases toward the southeast. The highly variable mor-

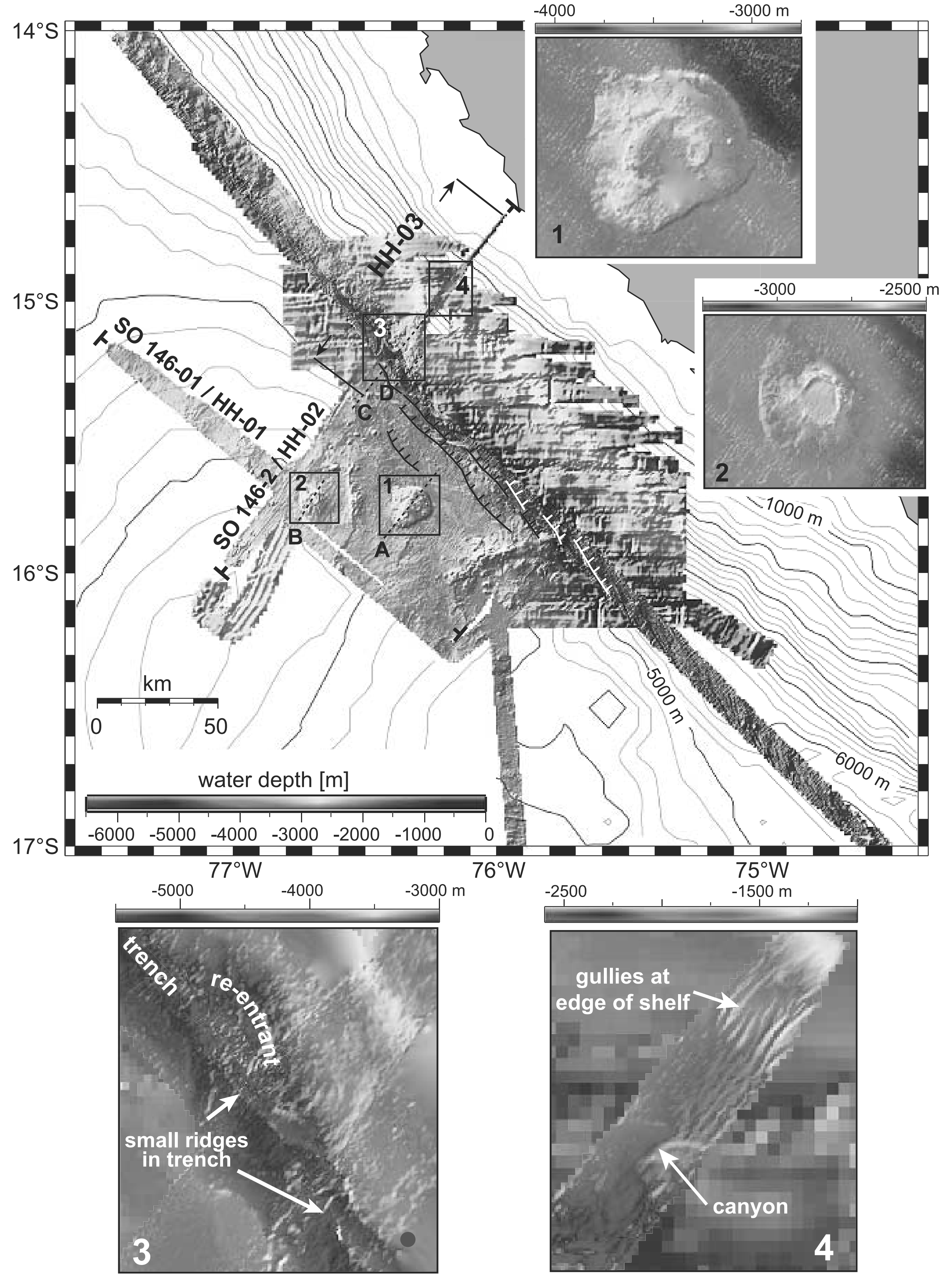

Figure 3. Bathymetric map compiled from Hydrosweep and SEAMARC II data. Numbered boxes refer to sections shown in insets. Dashed lines mark the locations of bathymetric profiles shown in Figure 4. Note the normal faults striking parallel to the trench. Red circle (inset 3) marks drilling site described by *Kulm et al.* [1974]. See color version of this figure in the HTML.

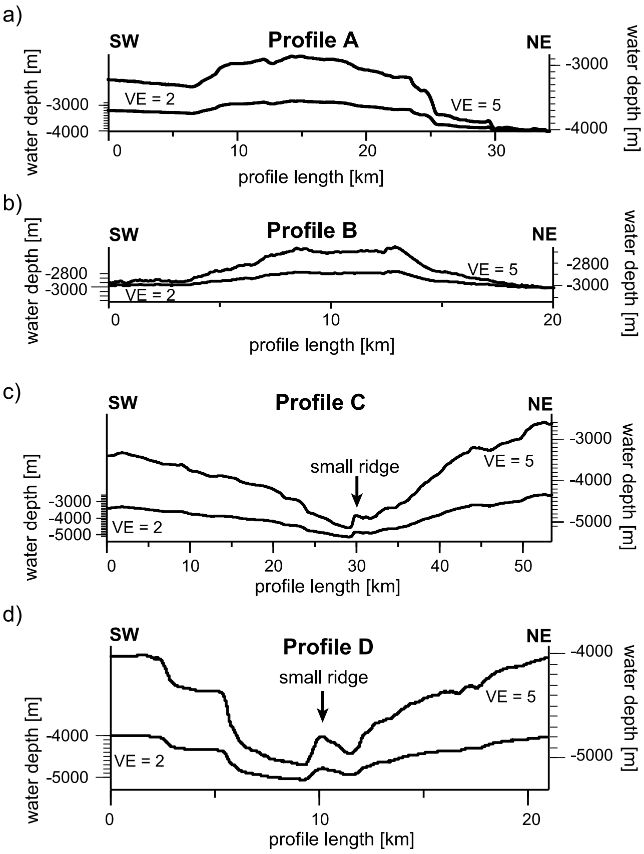

Figure 4. Bathymetric profiles across (a) seamount in the middle of the mapped area, (b) seamount with caldera, and (c) and (d) small ridges in the trench. For locations of profiles, see Figure 3.

phology of layer B_{oc}, e.g., the highs near stations OBH04 and OBH06, is reflected by undulations with increasingly longer wavelengths in layers C_{oc}–E_{oc}. The crustal structure of the Nazca Ridge observed beneath the crest in line SO146-01 shows no significant variations along the ridge axis, as imaged by the seismic profile SO146-02 along the ridge crest (Figure 9). Beneath the ridge axis, the Moho is located ~20 km below sea level, whereas it lies at ~18 km and ~16 km below sea level beneath the northwestern and southeastern ends of the profile, respectively.

[15] Taking into account the water depth, the crustal thickness of the ridge is ~17 km beneath the crest and ~16 km and ~14 km below the northwestern and southeastern flanks, respectively. Therefore the Nazca Ridge has a crustal root that is slightly asymmetrical with respect to the ridge crest (Figure 9). Despite the presence of the root, the ridge produces positive free-air anomalies; thus it is not completely isostatically compensated (Figure 13).

4.2. Structure of the Collision Zone

[16] Within ~20 km of the trench, the Nazca Ridge does not seem to undergo major deformation that can be linked to collision with the margin. At this distance, bending of the plate into the subduction zone leads to trench-parallel normal faults that increase in number as the trench is approached (Figures 3 and 6a). The normal faults have vertical offsets as high as 200 m (Figure 6a). At the collision zone, the ridge does not alter the curvature of the trench line. The water depth along the trench axis decreases from more than 6500 m south of the ridge to 5000 m above the ridge crest, a difference that equals the relief of the ridge.

[17] The sedimentary fill of the trench does not exceed 400 m and the gravity minimum associated with the trench axis is narrow (Figure 13). In the deepest part of the trench, two ~300-m-high and 10- to 15-km-long trench-parallel ridges exist that differ in their shape from the relief produced by normal faulting of the oceanic plate seaward of the trench axis (Figures 3 and 4). The one imaged in the seismic reflection section of Figure 6a is located above the subducting sediment pile, which does not appear to be deformed significantly. North of this small structural high, the water depth reaches a local maximum located in the middle of a 20-km-wide reentrant.

[18] Seismic profiles running along the ridge crest show the same thin layer of sediment as the lines that cross the ridge axis. The seismic reflection section shows that the ridge's sediment blanket seems to be completely subducted. In the velocity model derived from the wide-angle seismic data, the downgoing sediment layer cannot be resolved (Figure 9). The steep 9.5° dipping lower continental slope and the 4.4° dipping midslope exhibit a rough topography with structural highs and canyons (Figure 3). Up to the midslope, the sediment layer with a velocity of 1.6–1.8 km/s (A_{cont} in Figure 9) is only a few hundred meters thick. On the 2.4° dipping upper part of the midslope, two small sediment-filled basins 1 and 2 are present (Figure 9). Another ~1-km-thick sequence of sediments fills a depression of the basement (basin 3 in Figure 9) beneath the outer shelf along 10 km of profile SO146-02. Gullies present at ~2000 m water depth originate at the transition from the outer shelf to the upper slope (Figure 3, box 4). The uppermost sedimentary layer (A_{cont}) on the shelf is less than 100 m thick (Figure 9).

[19] Beneath layer A_{cont}, the upper plate consists of four layers (B_{cont}–E_{cont}) (Figure 9). Layers A_{cont} and B_{cont} are separated by an unconformity, imaged in the seismic reflection data (Figure 6c). B_{cont} with a velocity of 2.5–3.0 km/s is ~800 m thick and runs parallel to the seafloor from the trench to the midslope (OBS18). Between OBS18 and OBH22, this layer forms the structural highs separating the basins 1 and 2. C_{cont} has a downward increasing velocity of 3.5–4.0 km/s. Its thickness decreases landward from 2 km beneath the lower slope to 1 km at OBS18. D_{cont} that runs subparallel to the seafloor comprises velocities of 4.2–4.5 km/s, whereas the core of the continental wedge (E_{cont}) has velocities between 4.8 and 5.5 km/s. The free-air gravity across the continental slope shows a steep and relatively uniform gradient, but free-air anomalies ~10^{-5} m/s^2 occur along the coast (Figure 13).

[20] The Nazca plate can be traced to a submargin depth of ~28 km and an average angle of subduction of ~9°. In the subducted part of the ridge, seismic velocities and densities of the crustal layers increase by ~0.5–1.0 km/s and ~200 kg/m^3, respectively (Figures 9 and 13).

5. Discussion

5.1. Crustal Structure of the Nazca Ridge

[21] The surface of the Nazca Ridge lies, unlike the surrounding seafloor, above the carbonate compensation

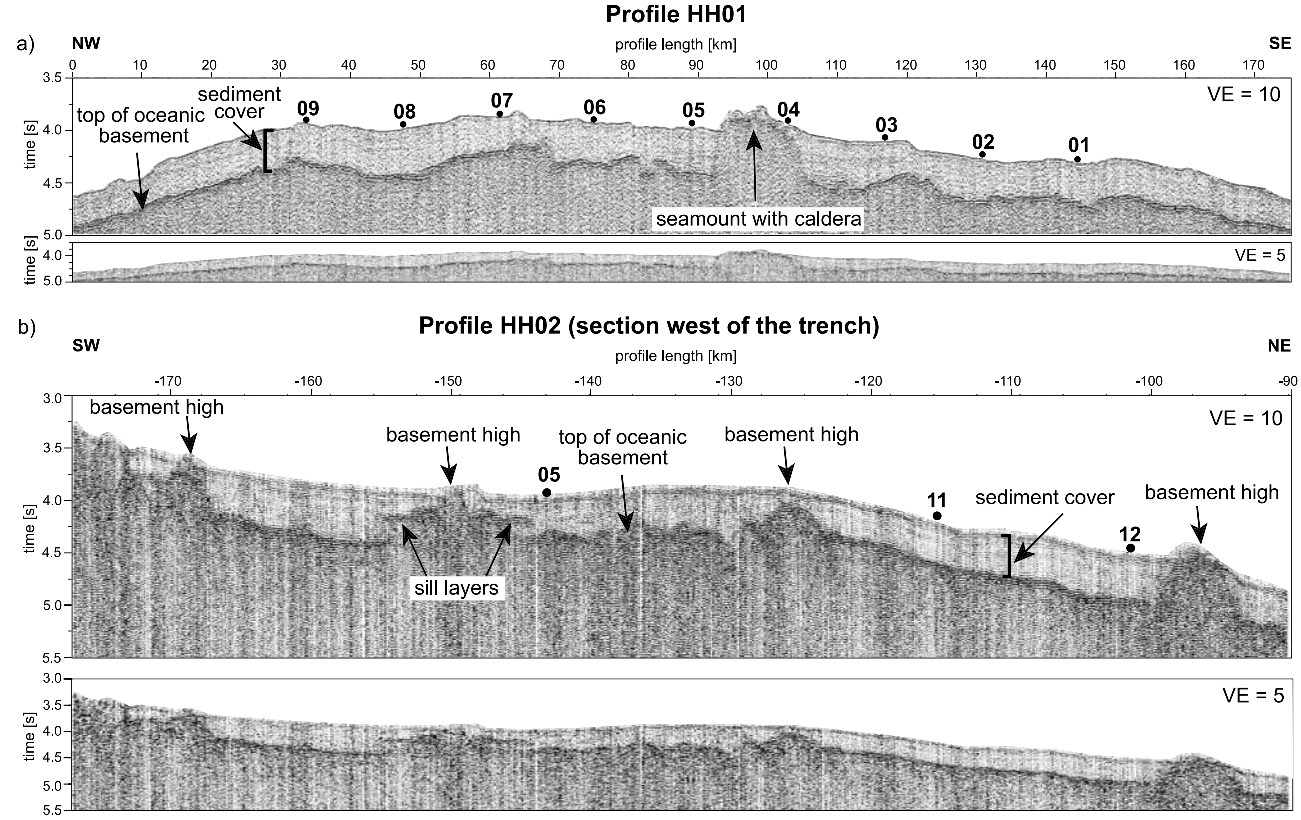

Figure 5. (a) Single-channel seismic reflection line HH-01 perpendicular to the ridge axis and (b) the part of single-channel line HH-02 located west of the trench running along the ridge crest. See Figure 2 for location.

depth (at 4000 m water depth) and thus a thin sediment cover of calcareous ooze overlies the igneous crust of the ridge [*Rosata and Kulm*, 1981]. The observed 300–400 m thickness of the sediment layer is confirmed by drilling on ODP Leg 202 site 1237 [*Shipboard Scientific Party*, 2002]. The sediment cover leads to a rather smooth topography of the southeastern flank for the Nazca Ridge, except where volcanic structures are located, compared to the rough relief of the surrounding Nazca plate north of the ridge [*Bialas and Kukowski*, 2000; *Kukowski et al.*, 2001b].

[22] The structure of the volcanic edifices on the ridge flank indicate a time lag between their formation and the formation of the main body of the ridge, because they look quite intact, e.g., the seamount with the preserved caldera (Figure 5a). This is consistent with the imaging of sill layers within the sedimentary cover [*Hagen and Moberly*, 1994] (Figure 5b). An off spreading axis origin is supported by the chemical composition of samples dredged on the small ridge located in the southeast corner of the mapped area (Figure 3) [*Hagen and Moberly*, 1994]. These samples were composed of mildly alkalic basaltic glass, which have considerably higher K_2O, Na_2O, and TiO_2 concentrations than normal mid-ocean ridge basalts [*Hagen and Moberly*, 1994]. The observation that the sediment cover on these features is thinner than the flanking basin floor may imply that sedimentation on tops of the volcanoes was limited for some time after their formation. A possible explanation for this could be that the tops of the volcanoes, which are now located at water depths of 2500–3000 m, may once have been near or above the sea level when the warm young crust of the Nazca Ridge was at lower water depth [*Detrick et al.*, 1977]. In this case, the tops of the volcanoes would have been affected by waves whose energy limited the deposition of sediment. Sedimentation might have started when the cooling Nazca Ridge, with the volcanoes on top, gradually sank to greater depths. Another possibility could be the presence of underwater currents flowing over the volcanic edifices, thereby preventing the deposition of a thick sediment cover.

[23] Seismic velocities of the crustal layers, as derived from wide-angle seismic data, are similar to those of typical oceanic crust [*Kennett*, 1982; *Mutter and Mutter*, 1993]. Thus the upper (B_{oc}, C_{oc}, D_{oc}) and lower (E_{oc}, F_{oc}) layers are interpreted to correspond to layers 2A, 2B, 2C, 3A, and 3B of typical oceanic crust, respectively (see Figure 9). The maximum thickness of 17 km of the ridge crust agrees with the value of 18 ± 3 km obtained by analyzing earthquake waves [*Woods and Okal*, 1994] and a thickness of 15 km inferred by interpretation of gravity data [*Couch and Whitsett*, 1981]. More than half of the crustal thickness of the ridge is contributed to by the lower crustal layer (F_{oc}), in agreement with observations for aseismic ridges worldwide [*Mutter and Mutter*, 1993]. Wide-angle seismic data constrain the presence of a slightly asymmetric crustal root with a steeper southeastern flank, as already indicated by *Couch and Whitsett*'s [1981] gravity model. Both velocity and gravity models suggest that the oceanic crust south of the ridge is 1–2 km thinner than north of it.

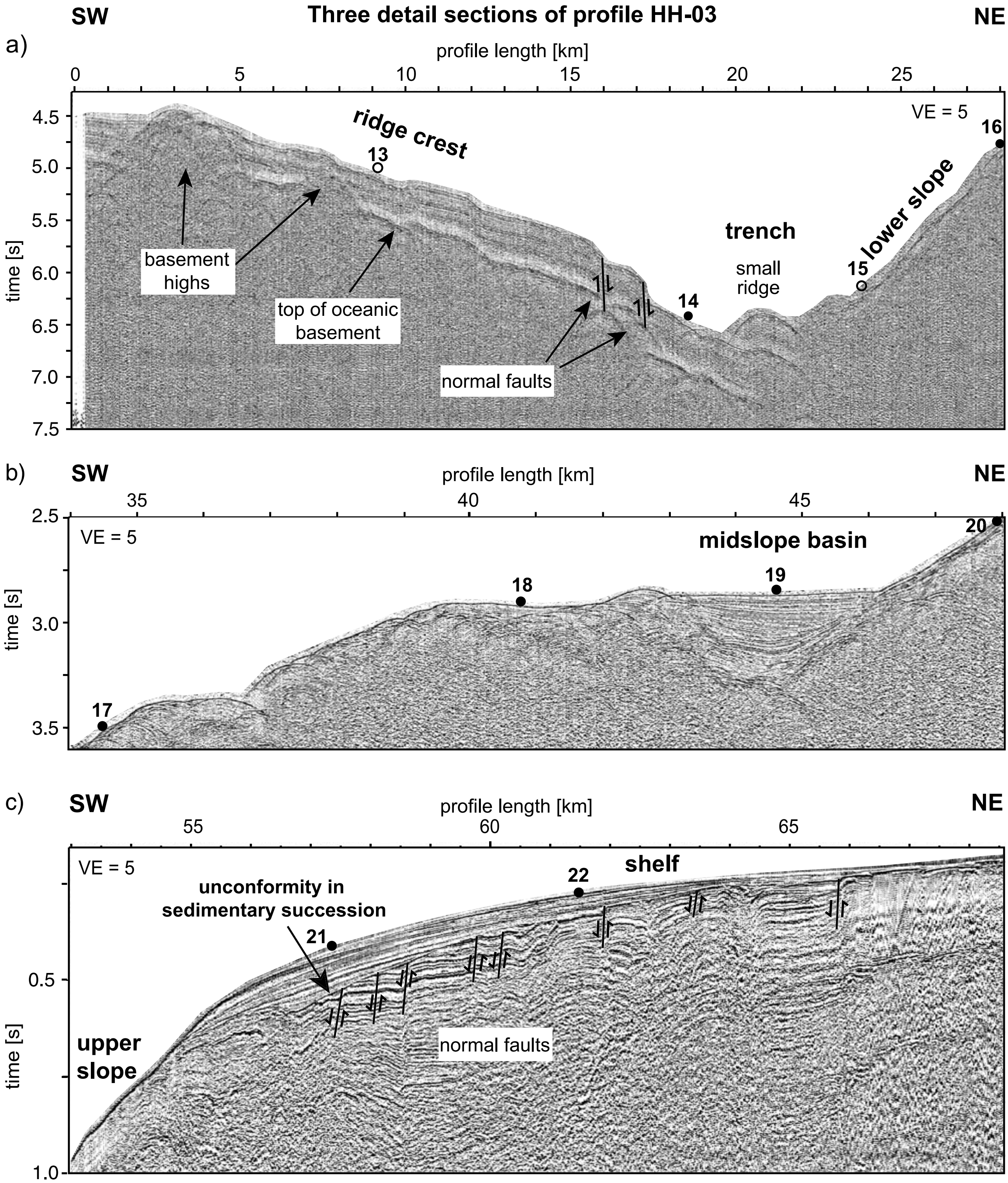

Figure 6. Three parts of stacked multichannel seismic line HH-03: (a) ridge crest, trench and lower slope (profile kilometer 0–28), (b) midslope basin (km 34–48), and (c) upper slope and shelf (km 50–69).

[24] The crustal structure of the Nazca Ridge is similar to aseismic ridges that originate at the intersection of a spreading center and a hot spot [*Talandier and Okal*, 1987; *Ito et al.*, 1995; *Corrigan et al.*, 1990; *Trummer et al.*, 2002; *Walther*, 2002]. These ridges share the characteristics that their thickness is caused by material accretion in the lower crust and that the proportion of layer 2 to layer 3 does not vary over a wide range [*Mutter and Mutter*, 1993].

5.2. Tectonic Erosion at the Collision Zone

[25] The presented data are consistent with the notion that the subduction of the Nazca Ridge causes enhanced tectonic erosion of the Peruvian forearc. In general, a dominating

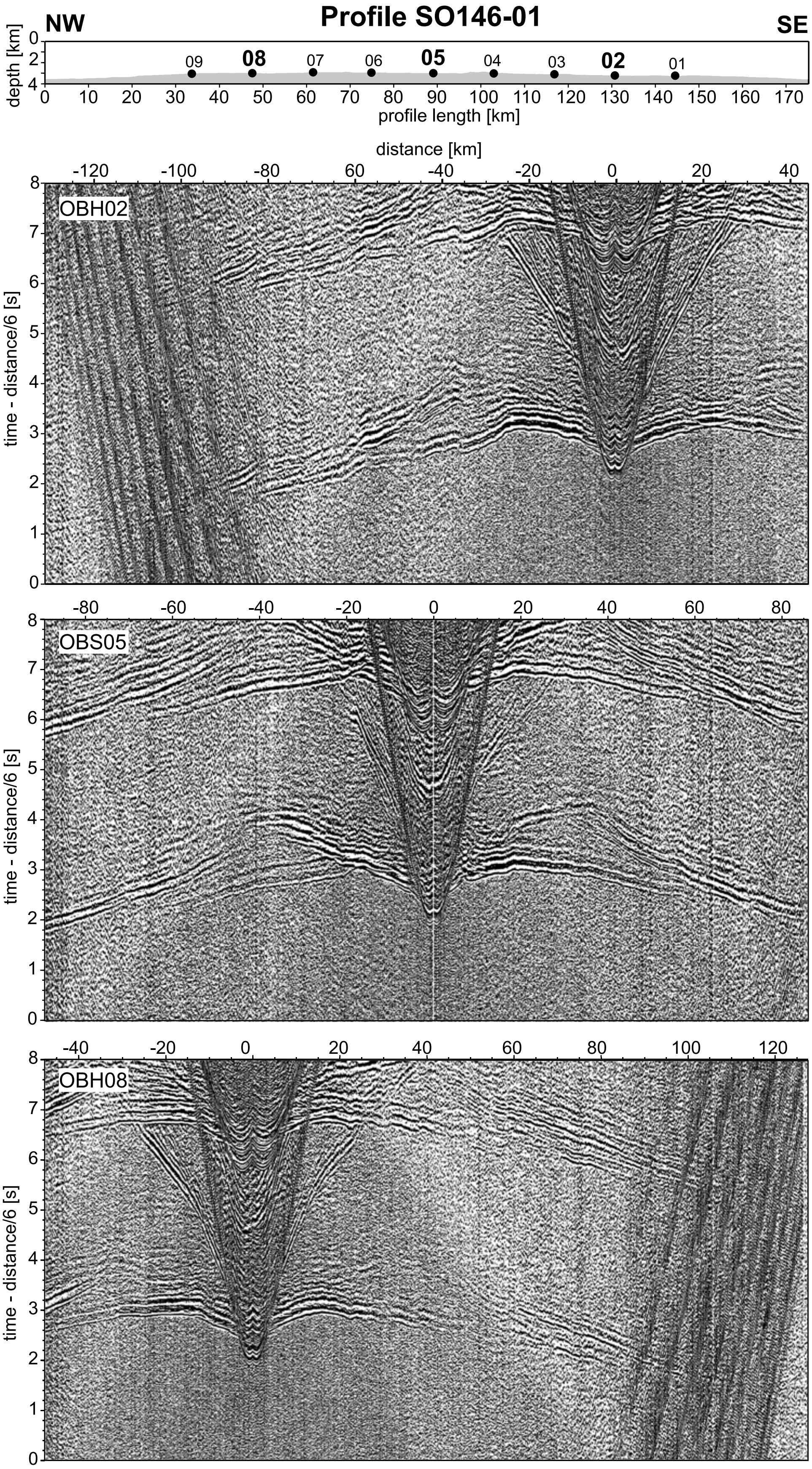

Figure 7. Example OBH record sections of the wide-angle seismic profile SO146-01 located perpendicular to the ridge axis. The sections are displayed time reduced by 6 km/s.

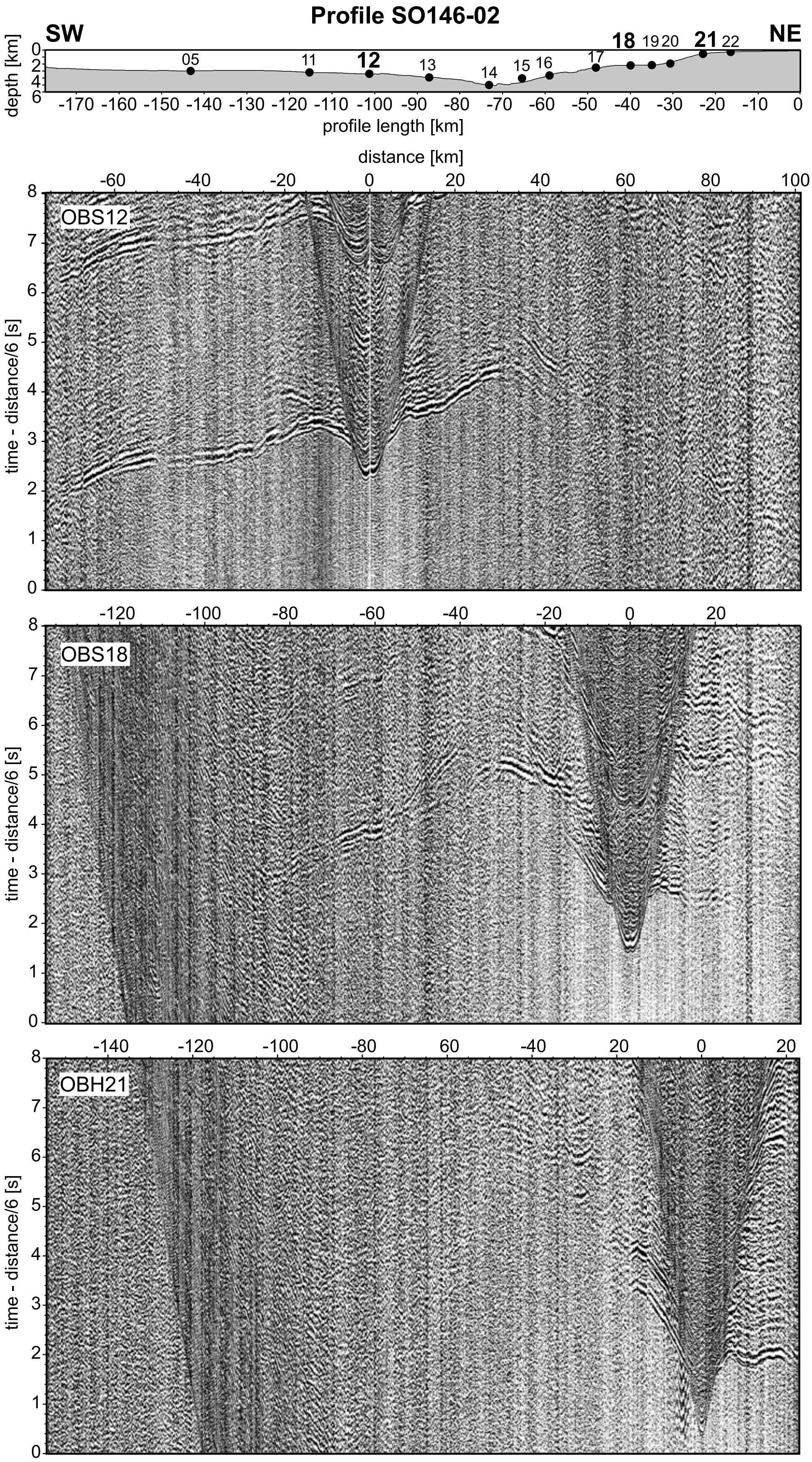

Figure 8. Example OBH record sections of the wide-angle seismic profile SO146-02 running along the ridge crest and extending toward the shelf. The sections are displayed time reduced by 6 km/s.

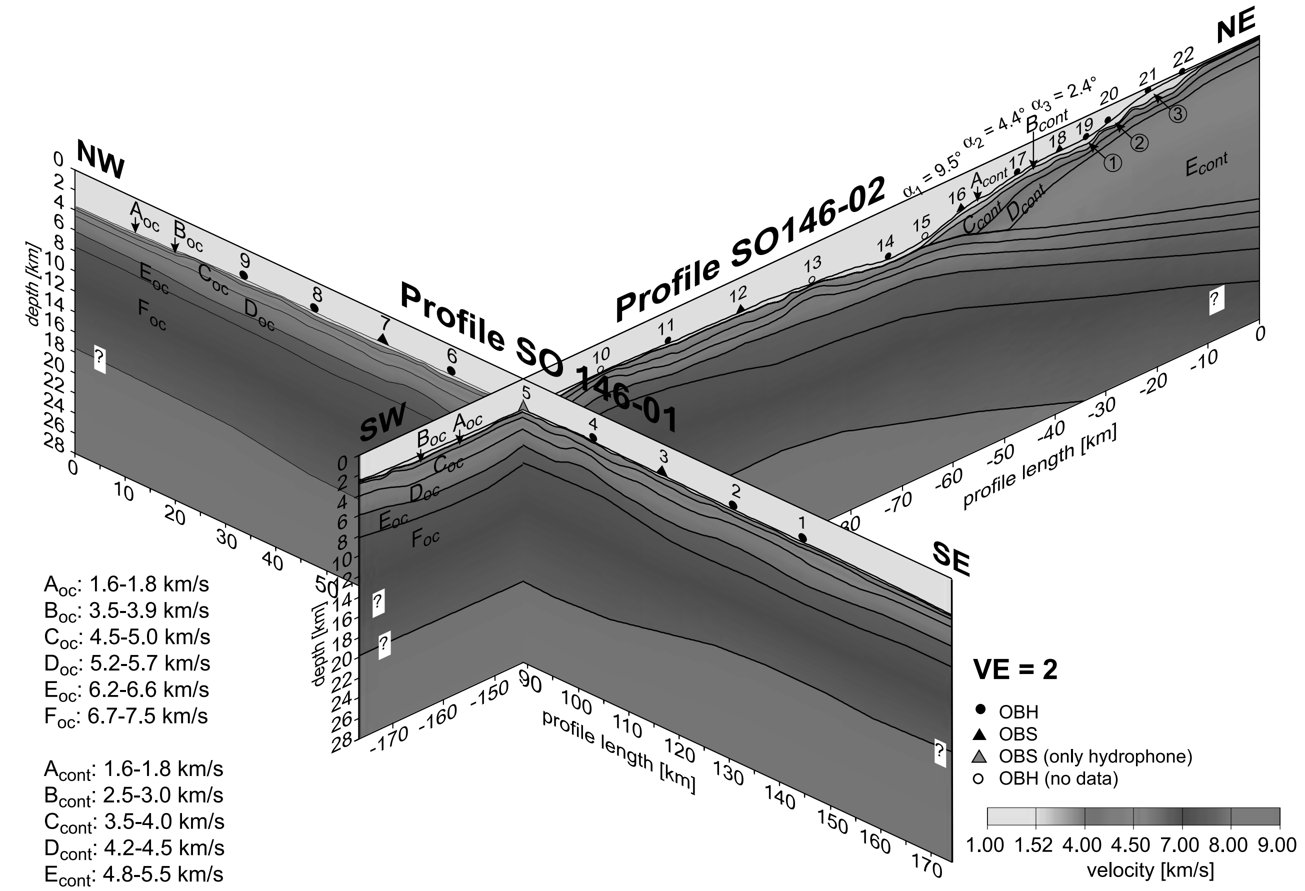

Figure 9. Velocity models for the wide-angle seismic profiles SO146-01 and SO146-02. Layers are correlated at station OBS05. For location of profiles see Figure 2. Three basins beneath the continental slope are labeled 1 to 3 (see section 4.2 for details). See color version of this figure in the HTML.

erosive regime can be inferred from a small sediment input from the oceanic plate, high seafloor roughness, a high forearc taper, high basal friction, a characteristic morphology, and internal structure of the forearc [*Scholl et al.*, 1980; *Hilde*, 1983; *Cloos and Shreve*, 1988a, 1988b; *Moore et al.*, 1986; *Ballance et al.*, 1989; *von Huene and Lallemand*, 1990; *von Huene and Scholl*, 1991; *Lallemand et al.*, 1992, 1994; *Clift and MacLeod*, 1999; *von Huene et al.*, 1999; *Vannucchi et al.*, 2001]. At erosive margins, in general, the slope of the upper plate is steep, irregular, and cut by numerous canyons and gullies indicating surface erosion, whereas the trench may be filled with debris from slumping [*Ranero and von Huene*, 2000; *Vanneste and Larter*, 2002; *von Huene and Ranero*, 2003]. In contrast to margins dominated by accretion, the slope at erosive margins is characterized by the lack of laterally continuous thrust ridges extending several tens to hundreds of kilometers along strike. The features indicative of ongoing tectonic erosion at the collision zone of the Nazca Ridge are discussed below.

[26] The important prerequisite of little sediment input to prevent massive accretion is provided by the Nazca Ridge, with its sedimentary cover not exceeding 400 m. The lack of a thick sedimentary cover contributes to seafloor roughness, which is further intensified by underthrusting of seamounts, volcanic ridges, and fault scarps. Accretive margins for example Makran, Cascadia or Nankai are underthrusted by oceanic crust buried beneath a thick sediment pile [*Moore and Biju-Duval*, 1984; *Davis and Hyndman*, 1989; *Minshull and White*, 1989; *Moore et al.*, 1990, 1995; *Kukowski et al.*, 2001a]. As revealed by our Peru seismic reflection data, the complete sequence of sediment on the Nazca Ridge is dragged beneath the toe of the continental slope (Figure 6a). Landward, the velocity model of wide-angle seismic line SO146-02 shows that the sediments are not accreted, but completely subducted. This is supported by the depositional history of the lowermost continental slope derived from drilled cores [*Kulm et al.*, 1974]. These cores show that calcareous ooze from the Nazca Ridge is an exotic constituent within the wedge and that these carbonates have been deposited by a slump event, which originated at the Nazca Ridge's crest [*Kulm et al.*, 1974].

[27] In the upper plate, the different layers of the velocity model show little lateral variation of the vertical velocity gradients. This is in contrast to velocity models for accretionary wedges, where typically velocities increase landward, owing to the gradual consolidation of accreted sediment [*Cochrane et al.*, 1994; *von Huene et al.*, 1994; *Carson and Westbrook*, 1995; *Flueh et al.*, 1998; *Kopp et*

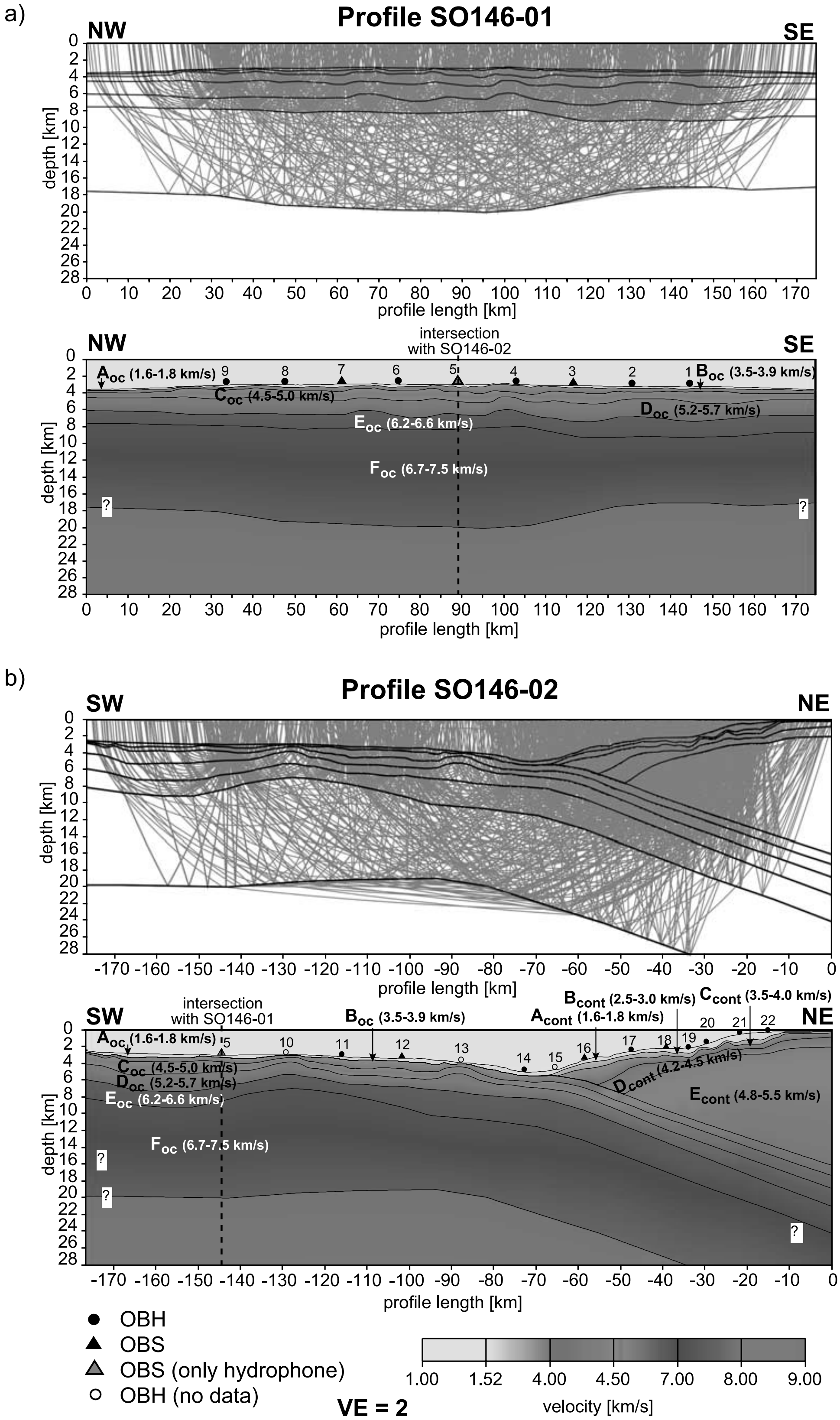

Figure 10. Ray coverage for the associated velocity fields obtained by forward modeling of the wide-angle seismic lines (a) SO146-01 and (b) SO146-02. The profiles intersect at station OBS05. See color version of this figure in the HTML.

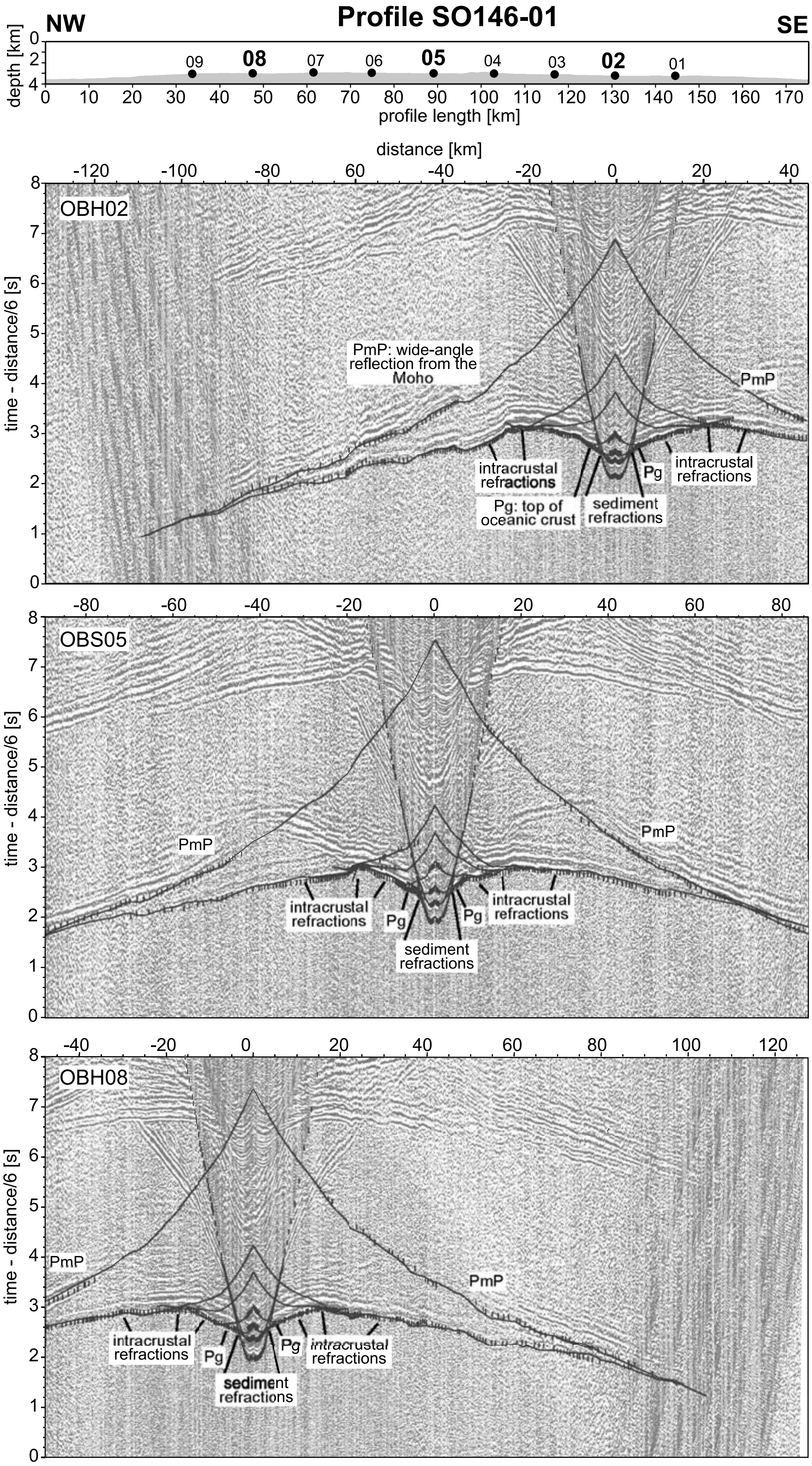

Figure 11. Interpretation of OBH record sections of profile SO146-01 shown with observed and calculated travel times obtained by two-dimensional ray tracing. *Pg* is refraction from the top of the oceanic crust; *PmP* is wide-angle reflection from the Moho.

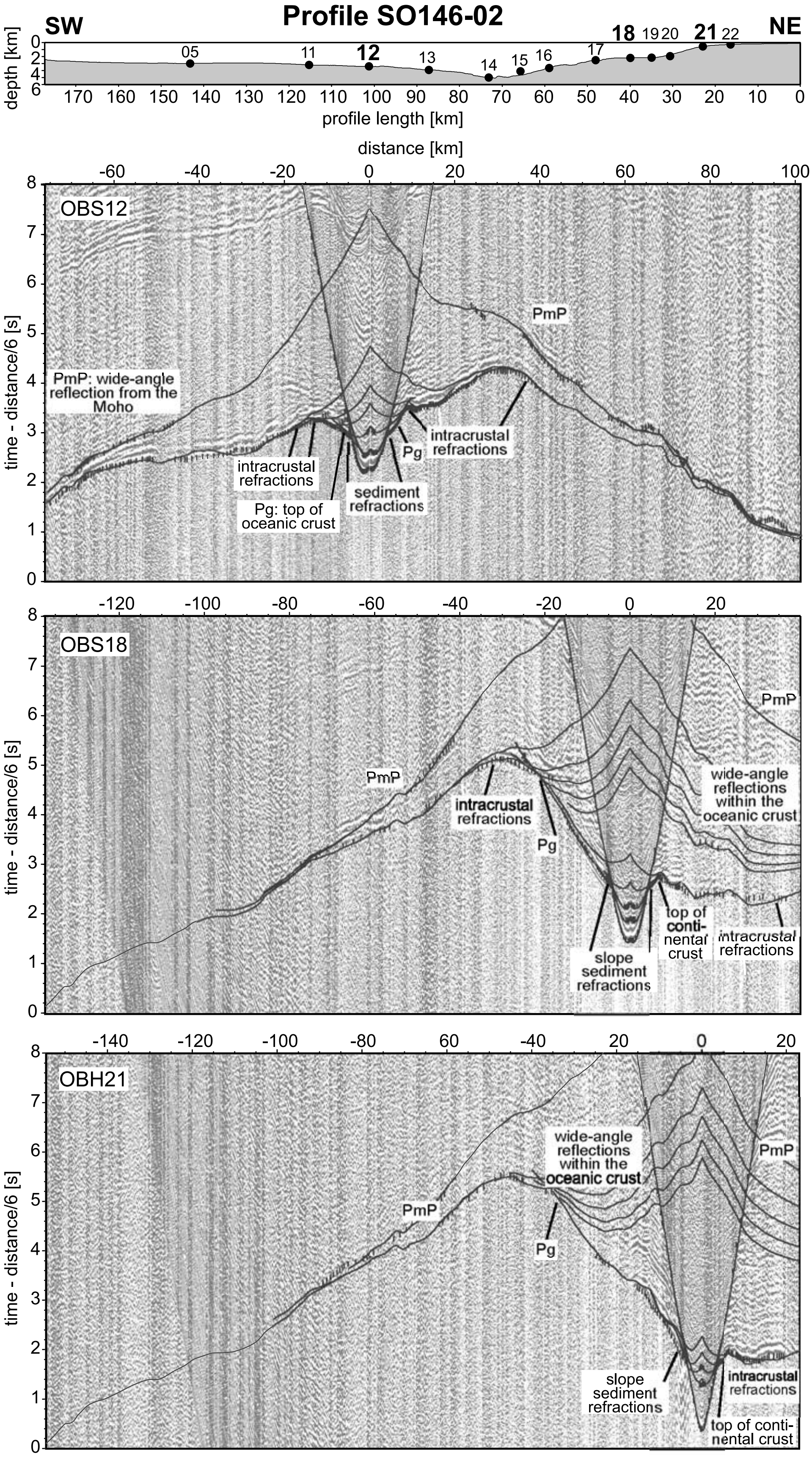

Figure 12. Interpretation of OBH record sections of profile SO146-02 shown with observed and calculated travel times obtained by two-dimensional ray tracing. *Pg* is refraction from the top of the oceanic crust; *PmP* is wide-angle reflection from the Moho.

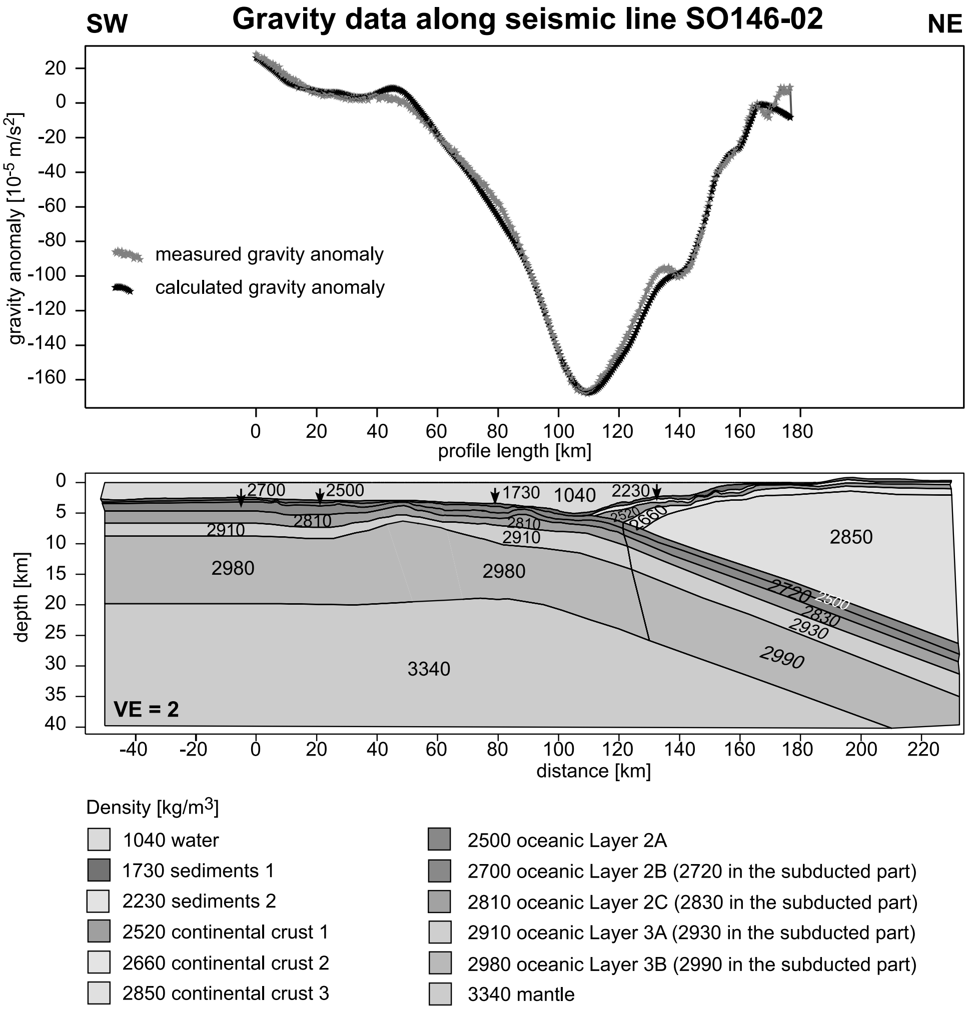

Figure 13. Observed and calculated gravity values and density model along seismic line SO146-02 located perpendicular to the trench. See color version of this figure in the HTML.

al., 2000; *Kopp et al.*, 2002]. The density model shows rocks with a relatively high density of 2520–2660 kg/m^3 700–1000 m below the seafloor, also arguing for the absence of a recently accreted sedimentary mass (Figure 13). Similar densities have been observed beneath the frontal part of the northern South Sandwich forearc that has been inferred to be primarily erosive [*Vanneste and Larter*, 2002].

[28] The only way to assess the type and age of the sedimentary units that constitute the forearc at the collision zone at 15°S is a correlation with seismic profiles and borehole data previously acquired north of the Nazca Ridge at 11.5°S, 9°S, and 5°S [*Kulm et al.*, 1981; *Suess et al.*, 1988, 1990]. Seismic reflection profiles in all three regions show a prominent, high-amplitude reflector, which is related to an unconformity between different sedimentary units and can been traced from the shelf to the upper part of the lower slope [*von Huene and Miller*, 1988]. This reflector seems to represent a regionally important seismic horizon apparently extending along the entire Peruvian forearc. In ODP Leg 112 cores at 11.5°S and 9°S, this reflector has been correlated with a prominent unconformity between Miocene sediment overlying Eocene strata [*Suess et al.*, 1988, 1990]. The Eocene strata, which overlie continental metamorphic rocks, were inferred to be deposited in a midshelf to upper slope environment [*Suess et al.*, 1988, 1990]. Under the assumption that the prominent seismic reflector observed north of the Nazca Ridge corresponds to the reflector observed in the seismic reflection data of the collision zone (Figure 6c), the reflection seismic horizons and the velocity model layers may be correlated with the drilled units of ODP Leg 112. It should be noted that such a correlation of drilled strata at 12°S and modeled layers at 15°S is not straightforward owing to the 500-km distance separating the Nazca Ridge and the ODP sites. In addition, the forearc at the collision zone has recently been uplifted by 1–2 km compared to the location of the drilling sites, as documented by the bathymetry data (Figure 3) and the elevation of Quaternary marine terraces [*Hsu*, 1992; *Macharé and Ortlieb*, 1992]. Assuming that a correlation is feasible, layer A_{cont} of the upper plate represents sedimentary units deposited since the Miocene. The unconformity between layer A_{cont} and layer B_{cont} might be equivalent to the unconformity at the base of the Miocene strata, whereas layers B_{cont} and C_{cont} would correspond to the Eocene strata overlying crystalline basement rocks (layer D_{cont}). This is supported by the seismic velocity of 4.2–4.5 km/s and the density of 2660 kg/m^3 observed for layer D_{cont}. This correlation would imply that Eocene midshelf to upper slope sediments are

located near the trench and that the crystalline core of the continental wedge extend as far seaward as 15 km from the trench (Figure 9). This interpretation is in agreement with the observation that rocks of high density and seismic velocities are located only a few kilometers landward of the trench (Figure 9). The presence of midshelf to upper slope sediment near the trench only at few hundred meters depth below seafloor would require a much longer time period of tectonic erosion than 2 Myr, the time span since the onset of ridge subduction at 15°S, and thus may be regarded as a piece of evidence for a long-term erosive regime.

[29] Another argument supporting an erosive regime is provided by the observation that a reentrant as wide as the Nazca Ridge is absent at the collision zone. How deep a ridge indents a forearc, may depend on the mechanical strength of the material of the continental wedge that, in turn, may be linked to the mass transfer regime. Rocks of high seismic velocity and density, which are present close to the trench, are likely to be mechanically strong. We envision that the strength of these rocks has prohibited a deep indentation of the wedge by the underthrusting ridge. A comparison with other margins experiencing ridge subduction shows that deep reentrants develop preferentially in settings where ridges underthrust accretionary prisms composed of mechanically weak rocks [*McCann and Habermann*, 1989; *Bouysse and Westercamp*, 1990; *Dominguez et al.*, 1998; *Schnuerle et al.*, 1998]. In contrast, the subduction of the Carnegie and Cocos Ridges at the erosive Ecuadorian and Costa Rican continental margins, respectively, does not lead to a significant indentation of the forearc [*McCann and Habermann*, 1989; *Corrigan et al.*, 1990; *Gutscher et al.*, 1999; *Collot et al.*, 2002]. At the Louisville Ridge, a chain of seamounts subducting at the Tonga margin, the largest arcward displacement of the plate boundary is observed at the northern edge of the southward migrating collision zone [*Vogt et al.*, 1976; *Ballance et al.*, 1989; *McCann and Habermann*, 1989; *Lallemand et al.*, 1994]. In conclusion, the Peruvian margin is similar to the Ecuadorian and Costa Rican subduction zones. Off Peru, reentrants of much smaller scale may be produced by the seamounts and volcanic ridges located on the Nazca Ridge when they collide with the upper plate. Such a small volcanic feature may have caused the 20-km-wide marginward deflection of the lower slope (Figure 3, box 3).

[30] Adjacent to this small reentrant, two 10- to 15-km-long, trench-parallel ridges described in Section 4.2 occur in the deepest part of the trench (Figures 3 and 6a). These features, which are exclusively found near the ridge crest, are asymmetric, with their seaward flanks being steeper than their landward flanks, and lie on top of the entire sedimentary cover of the Nazca Ridge. The observation that these ridges are separated by deep troughs from the toe of the wedge, makes the possibility that they constitute the frontal thrust slices of an accretionary prism unlikely (Figure 3). Instead, we suggest that the ridges are slump masses which, after deposition in the trench, have suffered limited shortening because of the landward directed drag induced by the underlying sediment layer of the subducting ridge. This interpretation is supported by drill cores obtained on the lowermost continental slope opposite to these ridges by piston and gravity corers (see Figure 3, box 3) [*Kulm et al.*, 1974; *Rosata and Kulm*, 1981; *Schweller et al.*, 1981]. These cores from a water depth of 4900 m document that two major slump events reached the lowermost continental slope within the last 400 000 years [*Kulm et al.*, 1974]. The older slump must have been derived from the continental margin because it contains Pliocene to Pleistocene calcareous ooze that formed under the influence of the cold Peru current. Later, a second slump transported Pliocene calcareous ooze and a basalt fragment from the crest of the Nazca Ridge to the toe of the continental margin. The different origin of the two types of calcareous ooze, one from the Nazca Ridge and the older one from the continental slope, are clear from their fossil contents [*Kulm et al.*, 1974]. The maximum age of 400 000 years for the two slumps, provided by radiolarian assemblages [*Kulm et al.*, 1974], may be used to place an upper age limit on the two ridges. If the ridges would be older the slump originating from the Nazca Ridge could not have reached the toe of the continental margin; instead it would have filled the deep trough SW of the ridges. As a consequence of this age constraint we consider the linear ridges to be transient features that ultimately will be dragged and subducted beneath the continental wedge (Figures 6a). Such underthrusting of erosional debris is known to be a characteristic mass transfer mode at erosive margins [*Scholl et al.*, 1980; *Cloos and Shreve*, 1988a, 1988b; *von Huene and Lallemand*, 1990; *Lallemand et al.*, 1994; *Vanneste and Larter*, 2002].

[31] A comparison with the forearc systems north of the Nazca Ridge [*Kukowski et al.*, 2001b; *Krabbenhoeft et al.*, 2003] shows that both the angle of the lower slope and the taper are largest at 15°S. The geological record at 9°S, where the ridge did not affect the margin, differs significantly from 11.5°S, where the ridge crest passed 9.5 Myr ago [*Hampel*, 2002], and the present collision zone at 15°S. Whereas the margin at 9°S has subsided more than 1000 m for 12–13 Myr, the region at 11.5°S has undergone a phase of uplift and enhanced tectonic erosion during 11–7 Ma with subsequent subsidence of more than several hundred meters since 6 Ma [*von Huene et al.*, 1988; *von Huene and Lallemand*, 1990; *Clift et al.*, 2003]. Erosion rates derived from subsidence reconstruction for the Lima Basin at 11.5°S show a rate 10 times higher during and shortly after the passage of the Nazca Ridge than before [*Clift et al.*, 2003].

[32] On the basis of these lines of argument, we suggest that tectonic erosion at the collision zone is more intense than off central Peru and that this observation can be attributed to the passage of the Nazca Ridge. We further speculate that tectonic erosion had long been the dominating mass transfer process before the ridge arrived. A look at the regions south of the Nazca Ridge would help to support this idea; however, few data are available off the adjacent Arica Bight [*Coulburn*, 1981]. However, it is known that the subduction zone setting does not change significantly around the Arica Bight, in particular, that the sediment cover on the Nazca plate is as thin as off Peru and north Chile [*von Huene et al.*, 1999; *Adam and Reuther*, 2000; *von Huene and Ranero*, 2003]. We propose that the geodynamic setting of the south Peruvian margin prior to the subduction of the ridge was characterized by a similar dominance of long-term subduction erosion as it is well documented at the north Chilean margin [*von Huene et al.*, 1999; *Adam and Reuther*, 2000; *von Huene and Ranero*,

2003]. In our view, the subduction of the Nazca Ridge causes enhanced, short-term tectonic erosion that is superposed on a long-term, primarily erosive regime.

6. Conclusions

[33] The GEOPECO geophysical survey revealed that the crust of the Nazca Ridge is built by layers of seismic velocities similar to that of typical oceanic crust. Owing to a considerably thicker layer 3, the ridge's total crustal thickness is ~17 km. The relative proportion of layer 2 to layer 3 is in agreement with observations from other aseismic ridges worldwide formed at the intersection of spreading centers and hot spots.

[34] The collision zone of the Nazca Ridge at 15°S shows characteristics of a margin undergoing tectonic erosion, which include, among others, a small sediment input, a high taper of the continental wedge indicating high basal friction, and the presence of rocks with high seismic velocities and densities near the trench. Correlation of modeled layers from a well-constrained velocity model with ODP Leg 112 stratigraphy north of the ridge suggests that shelf deposits overlying the crystalline basement of the continental wedge extend close to the trench. The presence of mechanically strong material extending almost to the trench explains why the subduction of the ridge does not lead to a marginward indentation or deflection of the trench. We propose that the tectonic erosion caused by the Nazca Ridge intensifies a long-term erosive regime, inferred for southern Peru by a comparison with the central Peruvian margin.

[35] **Acknowledgments.** We are grateful to Capt. Papenhagen and his crew for their excellent support during the SO146-GEOPECO cruise and to all participants of the cruise for their committed work during data acquisition and processing. Thanks to H.-J. Goetze and S. Schmidt for providing the IGMAS program and to G. Moore for making the bathymetry data of the R/V *Moana Wave* cruises MW8709 and MW8710 of the former Hawaii Institute of Geophysics available. One of us (A.H.) wishes to thank R. Hetzel for helpful constructive criticism on several earlier versions of the manuscript. The GMT software by P. Wessel and W. H. Smith was used to create most of the figures. We thank the Associate Editor D. Sandwell and reviewers D. Scholl and G. Moore for their detailed and constructive comments. Funding was provided by the German Ministry of Education, Science and Technology (BMBF) for the GEOPECO project (grant 03G0146A) and to one of us (A.H.) by the Deutsche Forschungsgemeinschaft (DFG) through a grant (Leibniz-Program) to O. Oncken.

References

Adam, J., and C.-D. Reuther (2000), Crustal dynamics and active fault mechanics during subduction erosion: Application of frictional wedge analysis on the North Chilean Forearc, *Tectonophysics*, *321*, 297–325.

Ballance, P. F., D. W. Scholl, T. L. Vallier, A. J. Stevenson, H. Ryan, and R. H. Herzer (1989), Subduction of a Late Cretaceous seamount of the Louisville Ridge at the Tonga Trench: A model of normal and accelerated tectonic erosion, *Tectonics*, *8*, 953–962.

Behrmann, J., and A. Kopf (2001), Balance of tectonically accreted and subducted sediment at the Chile Triple Junction, *Geol. Rundsch.*, *90*, 753–768.

Bialas, J., and E. R. Flueh (1999), Ocean bottom seismometers, *Sea Technol*, *40*, 41–46.

Bialas, J., and N. Kukowski (2000), Geophysical experiments at the Peruvian continental margin; investigations of tectonics, mechanics, gas hydrates and fluid transport, *GEOMAR Rep. 96*, Geomar, Kiel, Germany.

Bouysse, P., and D. Westercamp (1990), Subduction of Atlantic aseismic ridges and Late Cenozoic evolution of the Lesser Antilles island arc, *Tectonophysics*, *175*, 349–380.

Cande, S. C. (1984), Nazca-South American plate interactions since 50 mybp, in *Atlas of the Ocean Margin Program*, vol. VI, *Peru Continental Margin*, edited by D. M. Hussong et al., p. 14, Mar. Sci. Int., Woods Hole, Mass.

Caress, D. W., and D. N. Chayes (1995), New software for processing sidescan data form sidescan-capable multibeam sonars, in *Proceedings of the IEEE Oceans 95 Conference*, pp. 997–1000, Mar. Technol. Soc., Washington, D. C.

Carson, B., and G. K. Westbrook (1995), Modern fluid flow in the Cascadia accretionary wedge: A synthesis, *Proc. Ocean Drill. Program Sci. Results*, *146*, part 1, 413–421.

Chung, W. Y., and H. Kanamori (1978), A mechanical model for plate deformation associated with aseismic ridge subduction in the New Hebrides Arc, *Tectonophysics*, *50*, 29–40.

Clift, P. D., and C. J. MacLeod (1999), Slow rates of subduction erosion estimated from subsidence and tilting of the Tonga forearc, *Geology*, *27*, 411–414.

Clift, P. D., I. Pecher, N. Kukowski, and A. Hampel (2003), Tectonic erosion of the Peruvian Forearc, Lima Basin, by subduction and Nazca Ridge collision, *Tectonics*, *22*(3), 1023, doi:10.1029/2002TC001386.

Cloos, M. (1993), Lithospheric buoyancy and collisional orogenesis: Subduction of oceanic plateaus, continental margins, island arcs, spreading ridges and seamounts, *Geol. Soc. Am. Bull.*, *105*, 715–737.

Cloos, M., and R. L. Shreve (1988a), Suduction-channel model of prism accretion, melange formation, sediment subduction, and subduction erosion at convergent plate margins; Part I, Background and description, *Pure Appl. Geophys.*, *128*, 455–500.

Cloos, M., and R. L. Shreve (1988b), Suduction-channel model of prism accretion, melange formation, sediment subduction, and subduction erosion at convergent plate margins; Part II, Implications and discussion, *Pure Appl. Geophys.*, *128*, 501–545.

Cochrane, G. R., J. C. Moore, M. E. MacKay, and G. F. Moore (1994), Velocity-inferred porosity model of the Oregon Accretionary Prism from multichannel seismic reflection data, *J. Geophys. Res.*, *99*, 7033–7045.

Collot, J.-Y., and B. Davy (1998), Forearc structures and tectonic regimes at the oblique subduction zone between the Hikurangi Plateau and the southern Kermadec margin, *J. Geophys. Res.*, *103*, 623–650.

Collot, J.-Y., and M. A. Fisher (1991), The collision zone between the North d'Entrecasteaux ridge and the New Hebrides island arc: 1. Sea Beam morphology and shallow structure, *J. Geophys. Res.*, *96*, 4479–4495.

Collot, J.-Y., P. Charvis, M. A. Gutscher, and S. Operto (2002), Exploring the Ecuador-Colombia active margin and interplate seismogenic zone, *Eos Trans. AGU*, *83*(17), 185, 189–190.

Corrigan, J., P. Mann, and J. C. Ingle (1990), Forearc response to subduction of the Cocos Ridge, Panama-Costa Rica, *Geol. Soc. Am. Bull.*, *102*, 628–652.

Couch, R., and R. M. Whitsett (1981), Structures of the Nazca Ridge and the continental shelf and slope of southern Peru, in *Nazca Plate: Crustal Formation and Andean Convergence*, edited by L. D. Kulm et al., *Mem. Geol. Soc. Am.*, *154*, 569–586.

Coulburn, W. T. (1981), Tectonics of the Nazca plate and the continental margin of western South America, 18°S to 23°S, in *Nazca Plate: Crustal Formation and Andean Convergence*, edited by L. D. Kulm et al., *Mem. Geol. Soc. Am.*, *154*, 587–618.

Davis, E. E., and R. D. Hyndman (1989), Accretion and recent deformation of sediments along the northern Cascadia subduction zone, *Geol. Soc. Am. Bull.*, *101*, 1465–1480.

Detrick, R. S., J. G. Sclater, and J. Thiede (1977), The subsidence of aseismic ridges, *Earth Planet. Sci. Lett.*, *34*, 185–196.

Dominguez, S., S. Lallemand, J. Malavieille, and P. Schnuerle (1998), Oblique subduction of the Gagua Ridge beneath the Ryukyu accretionary wedge system: Insights from marine observations and sandbox experiments, *Mar. Geophys. Res.*, *20*, 383–402.

Dupont, J. (1982), Morphologie et structures superficielles del'arc des Tonga-Kermadec, *Contrib. Etude Geodyn. Sud-Ouest Pac. 147*, pp. 263–282, ORSTOM, Paris.

Dupont, J., and R. H. Herzer (1985), Effect of subduction of the Louisville Ridge on the structure and morphology of the Tonga Arc, in *Geology and Offshore Resources of Pacific Island Arcs-Tonga Region*, *Earth Sci. Ser.*, vol. 2, edited by D. W. Scholl and T. L. Vallier, pp. 323–334, Circum-Pac. Counc. for Energy and Miner. Resour., Houston, Tex.

Fisher, M. A., J.-Y. Collot, and E. L. Geist (1991), The collision zone between the North d'Entrecasteaux ridge and the New Hebrides island arc: 2. Structure from multichannel seismic data, *J. Geophys. Res.*, *96*, 4470–4495.

Flueh, E. R., and J. Bialas (1996), A digital, high data capacity ocean bottom recorder for seismic investigations, *Int. Underwater Syst. Design*, *18*, 18–20.

Flueh, E. R., et al. (1998), New seismic images of the Cascadia subduction zone from cruise SO108-ORWELL, *Tectonophysics*, *293*, 69–84.

Gardner, T. W., D. Verdonck, N. M. Pinter, R. Slingerland, K. P. Furlong, T. F. Bullard, and S. G. Wells (1992), Quaternary uplift astride the aseismic Cocos Ridge, Pacific coast, Costa Rica, *Geol. Soc. Am. Bull.*, *104*, 219–232.

Geist, E. L., and D. W. Scholl (1994), Large-scale deformation related to the collision of the Aleutian Arc with Kamchatka, *Tectonics*, *13*, 538–560.

Geist, E. L., M. A. Fisher, and D. W. Scholl (1993), Large-scale deformation associated with ridge subduction, *Geophys. J. Int.*, *115*, 344–366.

GEODAS (1992), Marine geological and geophysical data from U.S. Department of Commerce NOAA and NGDC [CD-ROM]. (Available at http://www.ngdc.noaa.gov/mgg/geodas/geodas.html)

Goetze, H.-J., and B. Lahmeyer (1988), Application of three-dimensional interactive modeling in gravity and magnetics, *Geophysics*, *53*, 1096–1108.

Grant, J. A., and R. Schreiber (1990), Modern swath sounding and sub-bottom profiling technology fro research applications: The Atlas Hydrosweep and Parasound systems, *Mar. Geophys. Res.*, *12*, 9–19.

Gutscher, M.-A., J. Malavieille, S. Lallemand, and J.-Y. Collot (1999), Tectonic segmentation of the North Andean margin: Impact of the Carnegie Ridge collision, *Earth Planet. Sci. Lett.*, *168*, 255–270.

Hagen, R. A., and R. Moberly (1994), Tectonic effects of a subducting aseismic ridge: The subduction of the Nazca Ridge at the Peru Trench, *Mar. Geophys. Res.*, *16*, 145–161.

Hampel, A. (2002), The migration history of the Nazca Ridge along the Peruvian active margin: A re-evaluation, *Earth Planet. Sci. Lett.*, *203*, 665–679.

Hilde, T. W. C. (1983), Sediment subduction versus accretion around the Pacific, *Tectonophysics*, *99*, 381–397.

Hsu, J. T. (1992), Quaternary uplift of the Peruvian coast related to the subduction of the Nazca Ridge: 13.5 to 15.6° south latitude, *Quat. Int.*, *15/16*, 87–97.

Hussong, D. M., T. B. Reed, and W. A. Bartlett (1988), SEAMARC II sonar imagery and bathymetry of the Nazca plate and forearc, ODP Leg 112, *Proc. Ocean Drill. Program Initial Rep.*, *112*, 125–130.

Ito, G., M. McNutt, and R. L. Gibson (1995), Crustal structure of the Tuamotu Plateau, 15°S, and implications for its origin, *J. Geophys. Res.*, *100*, 8097–8114.

Kennett, J. (1982), *Marine Geology*, Prentice-Hall, Old Tappan, N. J.

Kolarsky, R. A., P. Mann, and W. Montero (1995), Island arc response to shallow subduction of the Cocos Ridge, Costa Rica, in *Geologic and Tectonic Development of the Caribbean plate Boundary in Southern Central America*, edited by P. Mann, *Spec. Pap. Geol. Soc. Am.*, *295*, 235–262.

Kopp, C., J. Fruehn, E. R. Flueh, C. Reichert, N. Kukowski, J. Bialas, and D. Klaeschen (2000), Structure of the Makran subduction zone from wide-angle and reflection seismic data, *Tectonophysics*, *329*, 171–191.

Kopp, H., D. Klaeschen, E. R. Flueh, J. Bialas, and C. Reichert (2002), Crustal structure of the Java margin from seismic wide-angle and multichannel reflection data, *J. Geophys. Res.*, *107*(B2), 2034, doi:10.1029/2000JB000095.

Krabbenhoeft, A., J. Bialas, H. Kopp, N. Kukowski, and C. Huebscher (2003), Structure of the Peruvian continental margin: Results from wide-angle seismic data, *Geophys. Res. Abstr.*, 5Abstract 03848.

Kukowski, N., T. Schillhorn, K. Huhn, U. von Rad, S. Husen, and E. R. Flueh (2001a), Morphotectonics and mechanics of the central Makran accretionary wedge off Pakistan, *Mar. Geol.*, *173*, 1–19.

Kukowski, N., A. Hampel, J. Bialas, C. Huebscher, U. Barckhausen, and J. Bourgois (2001b), Tectonic erosion at the Peruvian margin: Evidence from swath bathymetry and process identification from 3D sandbox analogue modeling, *Eos Trans. AGU*, *82*(47), Fall Meet. Suppl., Abstract T31A-0817.

Kulm, L. D., J. M. Resig, T. C. Moore, and V. J. Rosato (1974), Transfer of Nazca Ridge pelagic sediments to the Peru continental margin, *Geol. Soc. Am. Bull.*, *85*, 769–780.

Kulm, L. D., J. Dymond, E. J. Dasch, and D. M. Hussong (1981), *Nazca Plate: Crustal Formation and Andean Convergence*, *Mem. Geol. Soc. Am.*, *154*, 834 pp.

Lallemand, S. E., J. Malavieille, and S. Calassou (1992), Effects of oceanic ridge subduction on accretionary wedges, experimental modeling and marine observations, *Tectonics*, *11*, 1301–1313.

Lallemand, S. E., P. Schnuerle, and J. Malavieille (1994), Coulomb theory applied to accretionary and nonaccretionary wedges: Possible causes for tectonic erosion and/or frontal accretion, *J. Geophys. Res.*, *99*, 12,033–12,055.

Laursen, J., D. W. Scholl, and R. von Huene (2002), Neotectonic deformation of the central Chile margin: Deepwater forearc basin formation in response to hot spot ridge and seamount subduction, *Tectonics*, *21*(5), 1038, doi:10.1029/2001TC901023.

LeFevre, L. V., and K. McNally (1985), Stress distribution and subduction of aseismic ridges in the Middle America subduction zone, *J. Geophys. Res.*, *90*, 4495–4510.

Lewis, S. D., et al. (1995), *Proceedings of the Ocean Drilling Program, Scientific Results*, vol. 141, 499 pp., Ocean Drill. Program, College Station, Tex.

Li, C., and A. L. Clark (1994), Tectonic effects of the subducting Nazca Ridge on the southern Peru continental margin, *Mar. Pet. Geol.*, *11*, 575–586.

Luetgert, J. H. (1992), MacRay-interactive two-dimensional seismic raytracing for the Macintosh, *U.S. Geol. Surv. Open File Rep.*, *92-356*, 43 pp.

Macharé, J., and L. Ortlieb (1992), Plio-Quarternary vertical motions and the subduction of the Nazca Ridge, central coast of Peru, *Tectonophysics*, *205*, 97–108.

McCann, W. R., and R. E. Habermann (1989), Morphologic and geologic effects of the subduction of bathymetric highs, *Pure Appl. Geophys.*, *129*, 41–69.

Minshull, T. A., and R. S. White (1989), Sediment compaction and fluid migration in the Makran accretionary prism, *J. Geophys. Res.*, *94*, 7387–7402.

Moore, G. F., T. H. Shipley, and P. Lonsdale (1986), Subduction erosion versus sediment offscraping at the toe of the Middle America Trench off Guatemala, *Tectonics*, *5*, 513–523.

Moore, G. F., T. H. Shipley, P. L. Stoffa, D. E. Karig, A. Taira, S. Kuramoto, H. Tokuyama, and K. Suyehiro (1990), Structure of the Nankai Trough accretionary zone from multichannel seismic reflection data, *J. Geophys. Res.*, *95*, 8753–8765.

Moore, J. C., and B. Biju-Duval (1984), Tectonic synthesis, Deep Sea Drilling Project Leg 78A: Structural evolution of offscraped and underthrust sediment, northern Barbados ridge complex, *Initial Rep. Deep Sea Drill. Proj.*, *78*, 601–621.

Moore, J. C., K. Moran, M. MacKay, and H. Tobin (1995), Frontal thrust, Oregon accretionary prism: Geometry, physical properties, and fluid pressure, *Proc. Ocean Drill. Program Sci. Results*, *146*, part 1, 3–31.

Mutter, C. Z., and J. C. Mutter (1993), Variations in thickness of layer 3 dominate oceanic crustal structure, *Earth Planet. Sci. Lett.*, *117*, 295–317.

Norabuena, E., L. Leffler-Griffin, A. Mao, T. Dixon, S. Stein, I. S. Sacks, L. Ocola, and M. Ellis (1998), Space geodetic observations of Nazca-South America convergence across the central Andes, *Science*, *279*, 358–362.

Pilger, R. H. (1981), Plate reconstructions, aseismic ridges, and low-angle subduction beneath the Andes, *Geol. Soc. Am. Bull.*, *92*, 448–456.

Pilger, R. H., and D. W. Handschumacher (1981), The fixed hotspot hypothesis and origin of the Easter-Salas y Gomez-Nazca trace, *Geol. Soc. Am. Bull.*, *92*, 437–446.

Ranero, C. R., and R. von Huene (2000), Subduction erosion along the Middle America convergent margin, *Nature*, *404*, 748–752.

Rosata, V. J., and L. D. Kulm (1981), Clay mineralogy of the Peru continental margin and adjacent Nazca plate: Implications for provenance, sea level changes, and continental accretion, in *Nazca Plate: Crustal Formation and Andean Convergence*, edited by L. D. Kulm et al., *Mem. Geol. Soc. Am.*, *154*, 545–568.

Rutland, R. W. R. (1971), Andean orogeny and ocean floor spreading, *Nature*, *233*, 252–255.

Schnuerle, P., C.-S. Liu, S. E. Lallemand, and D. L. Reed (1998), Structural insight into the south Ryukyu margin: Effects of the subducting Gagua Ridge, *Tectonophysics*, *288*, 237–250.

Scholl, D. W., M. N. Christensen, R. von Huene, and M. S. Marlow (1970), Peru-Chile Trench sediments and sea-floor spreading, *Geol. Soc. Am. Bull.*, *81*, 1339–1360.

Scholl, D. W., R. von Huene, T. L. Vallier, and D. G. Howell (1980), Sedimentary masses and concepts about tectonic processes at underthrust ocean margins, *Geology*, *8*, 564–568.

Schweller, W. J., L. D. Kulm, and R. A. Prince (1981), Tectonics, structure and sedimentary framework of the Peru-Chile trench, in *Nazca Plate: Crustal Formation and Andean Convergence*, edited by L. D. Kulm et al., *Mem. Geol. Soc. Am.*, *154*, 323–349.

Shipboard Scientific Party (2002), Leg 202, preliminary report, *ODP Prelim. Rep. 102*, Ocean Drill. Program, College Station, Tex. (Available from http://www-odp.tamu.edu/publications/prelim/202_prel/202PREL.PDF)

Smith, W. H. F., and D. T. Sandwell (1997), Global seafloor topography from satellite altimetry and ship depth soundings, *Science*, *277*, 1956–1962.

Spence, W., C. Mendoza, E. R. Engdahl, G. L. Choy, and E. Norabuena (1999), Seismic subduction of the Nazca Ridge as shown by the 1996–97 Peru earthquakes, *Pure Appl. Geophys.*, *154*, 753–776.

Spikings, R. A., W. Winkler, D. Seward, and R. Handler (2001), Along-strike variations in the thermal and tectonic response of the continental Ecuadorian Andes to the collision with heterogeneous oceanic crust, *Earth Planet. Sci. Lett.*, *186*, 57–73.

Suess, E., et al. (1988), *Proceedings of the Ocean Drilling Program, Initial Reports*, vol. 112, Ocean Drill. Program, College Station, Tex.
Suess, E., et al. (1990), *Proceedings of the Ocean Drilling Program, Scientific Results*, vol. 112, Ocean Drill. Program, College Station, Tex.
Swenson, J., and S. Beck (1999), Source characteristics of the 12 November 1996 M_w 7. 7 Peru subduction zone earthquake, *Pure Appl. Geophys.*, *154*, 731–751.
Talandier, J., and E. A. Okal (1987), Crustal structure in the Society and Tuamotu Islands, French Polynesia, *Geophys. J. R. Astron. Soc.*, *88*, 499–528.
Trummer, I., E. R. Flueh, and the Paganini Working Group (2002), Seismic constraints on the crustal structure of Cocos Ridge off the coast of Costa Rica, *Neues Jahrb. Geol. Paleontol. Abh.*, *255*, 25–37.
Vanneste, L. E., and R. D. Larter (2002), Sediment subduction, subduction erosion, and strain regime in the northern South Sandwich forearc, *J. Geophys. Res.*, *107*(B7), 2149, doi:10.1029/2001JB000396.
Vannucchi, P., D. W. Scholl, M. Meschede, and K. McDougall-Reid (2001), Tectonic erosion and consequent collapse of the Pacific margin of Costa Rica: Combined implications from ODP Leg 170, seismic offshore data, and regional geology of the Nicoya Peninsula, *Tectonics*, *20*, 649–668.
Vogt, P. R., A. Lowrie, D. R. Bracey, and R. N. Hey (1976), Subduction of aseismic oceanic ridges: Effects on shape, seismicity and other characteristics of consuming plate boundaries, *Spec. Pap. Geol. Soc. Am.*, *172*.
von Huene, R., and S. Lallemand (1990), Tectonic erosion along the Japan and Peru convergent margins, *Geol. Soc. Am. Bull.*, *102*, 704–720.
von Huene, R., and J. Miller (1988), Migrated multichannel seismic-reflection records across the Peru continental margin, ODP Leg 112, *Proc. Ocean Drill. Program Initial Rep.*, *112*, 109–124.
von Huene, R., and C. R. Ranero (2003), Subduction erosion and basal friction along the sediment-starved convergent margin off Antofagasta, Chile, *J. Geophys. Res.*, *108*(B2), 2079, doi:10.1029/2001JB0001569.
von Huene, R., and D. W. Scholl (1991), Observations at convergent margins concerning sediment subduction, sediment erosion, and the growth of continental crust, *Rev. Geophys.*, *29*, 279–316.
von Huene, R., E. Suess, and Leg 112 Shipboard Scientific Party (1988), Ocean Drilling Program Leg 112, Peru continental margin: Part 1: Tectonic history, *Geology*, *16*, 934–938.
von Huene, R., D. Klaeschen, B. Cropp, and J. Miller (1994), Tectonic structure across the accretionary and erosional parts of the Japan Trench, *J. Geophys. Res.*, *99*, 22,349–22,361.
von Huene, R., I. Pecher, and M.-A. Gutscher (1996), Development of the accretionary prism along Peru and material flux after subduction of Nazca Ridge, *Tectonics*, *15*, 19–33.
von Huene, R., J. Corvalan, E. R. Flueh, K. Hinz, J. Korstgard, C. Ranero, and W. Weinrebe (1997), Tectonic control of the subducting Juan Fernandez Ridge on the Andean margin near Valparaiso, Chile, *Tectonics*, *16*, 474–488.
von Huene, R., W. Weinrebe, and F. Heeren (1999), Subduction erosion along the north Chile margin, *J. Geodyn.*, *27*, 345–358.
Walther, C. (2002), Crustal structure of the Cocos Ridge northeast of Cocos Island, Panama Basin, *Geophys. Res. Lett.*, *29*(20), 1986, doi:10.1029/2001GL014267.
Woods, T. M., and E. A. Okal (1994), The structure of the Nazca Ridge and Sala y Gomez seamount chain from dispersion of Rayleigh waves, *Geophys. J. Int.*, *117*, 205–222.
Zelt, C. A., and R. B. Smith (1992), Seismic traveltime inversion for 2-D crustal velocity structure, *Geophys. J. Int.*, *108*, 16–34.

J. Bialas, GEOMAR Research Center for Marine Geosciences, Wischhofstr. 1–3, D-24148 Kiel, Germany.

A. Hampel, Institute of Geological Sciences, University of Berne, Baltzerstr. 1, CH-3012 Berne, Switzerland. (andrea@geo.unibe.ch)

R. Heinbockel and C. Huebscher, Institut fuer Geophysik, Universitaet Hamburg, Bundesstr. 55, D-20146 Hamburg, Germany.

N. Kukowski, GeoForschungsZentrum Potsdam, Telegrafenberg, D-14473 Potsdam, Germany.